Evaluation of tumorigenic potential of CeO$_2$ and Fe$_2$O$_3$ engineered nanoparticles by a human cell *in vitro* screening model

Todd A. Stueckle[a,b,*], **Donna C. Davidson**[a], **Raymond Derk**[a], **Tiffany G. Kornberg**[a,b], **Diane Schwegler-Berry**[a], **Sandra V. Pirela**[c], **Glen Deloid**[c], **Philip Demokritou**[c], **Sudjit Luanpitpong**[d], **Yon Rojanasakul**[b], and **Liying Wang**[a]

[a]HELD, National Institute for Occupational Safety and Health, Morgantown WV, 26505
[b]Department of Pharmaceutical Sciences, West Virginia University, Morgantown WV, 26506
[c]Center for Nanotechnology and Nanotoxicology, Harvard T. H. Chan School of Public Health, Boston MA [d]Siriraj Center of Excellence for Stem Cell Research, Faculty of Medicine Siriraj Hospital, Mahidol University, Bangkok 10700, Thailand

Abstract

With rapid development of novel nanotechnologies that incorporate engineered nanomaterials (ENMs) into manufactured products, long-term, low dose ENM exposures in occupational settings is forecasted to occur with potential adverse outcomes to human health. Few ENM human health risk assessment efforts have evaluated tumorigenic potential of ENMs. Two widely used nano-scaled metal oxides (NMOs), cerium oxide (nCeO$_2$) and ferric oxide (nFe$_2$O$_3$) were screened in the current study using a sub-chronic exposure to human primary small airway epithelial cells (pSAECs). Multi-walled carbon nanotubes (MWCNT), a known ENM tumor promoter, was used as a positive control. Advanced dosimetry modeling was employed to ascertain delivered *vs.* administered dose in all experimental conditions. Cells were continuously exposed *in vitro* to deposited doses of 0.18 μg/cm^2 or 0.06 μg/cm^2 of each NMO or MWCNT, respectively, over 6 and 10 weeks, while saline- and dispersant-only exposed cells served as passage controls. Cells were evaluated for changes in several cancer hallmarks, as evidence for neoplastic transformation. At 10 weeks, nFe$_2$O$_3$- and MWCNT-exposed cells displayed a neoplastic-like transformation phenotype with significant increased proliferation, invasion and soft agar colony formation ability compared to controls. nCeO$_2$-exposed cells showed increased proliferative capacity only. Isolated nFe$_2$O$_3$ and MWCNT clones from soft agar colonies retained their respective neoplastic-like phenotypes. Interestingly, nFe$_2$O$_3$-exposed cells, but not MWCNT cells, exhibited immortalization and retention of the neoplastic phenotype after repeated passaging (12 – 30 passages) and after cryofreeze and thawing. High content screening and protein expression analyses in acute exposure ENM studies *vs.* immortalized nFe$_2$O$_3$ cells, and isolated ENM clones, suggested that long-term

[*]Corresponding Author: Todd A. Stueckle, tstueckle@cdc.gov, Phone: 304 285-6098.

exposure to the tested ENMs resulted in iron homeostasis disruption, an increased labile ferrous iron pool, and subsequent reactive oxygen species generation, a well-established tumorigenesis promotor. In conclusion, sub-chronic exposure to human pSAECs with a cancer hallmark screening battery identified nFe_2O_3 as possessing neoplastic-like transformation ability, thus suggesting that further tumorigenic assessment is needed.

Graphical Abstract
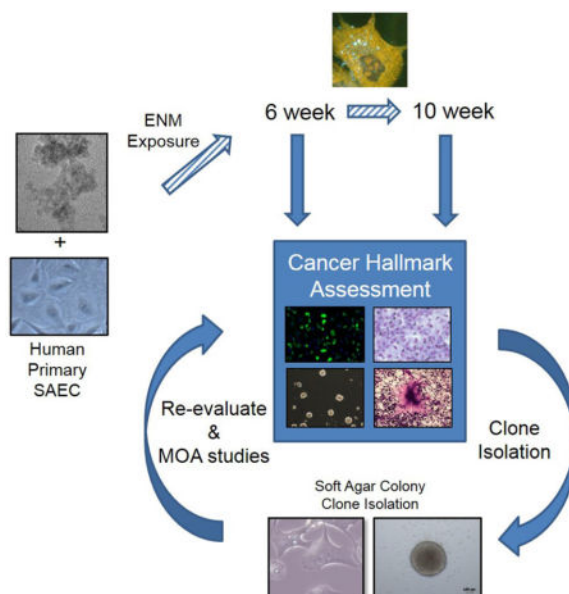
Keywords

nanomaterial; nano-scaled metal oxide; neoplastic transformation; iron homeostasis; tumorigenesis

1. Introduction

Incorporation of engineered nanomaterials (ENMs) into nanotechnology applications has reached far across numerous fields including industry, household products, commerce, and healthcare [1,2]. For example, current estimates place the nanotechnology industry with 6 million workers and a projected $3 trillion value by 2020 [3]. Along with the numerous benefits from nanotechnology development, concern about potential adverse effects to human and environmental health have arisen [4]. ENMs possess unique physicochemical properties, such as high surface-to-volume ratio, which impart unique, but somewhat unpredictable effects once exposed to biological systems. Several inhaled ENMs, including MWCNT, show unique toxicokinetics, biopersistence, and adverse effects inclusive of epigenetic alterations in exposed lung and extrapulmonary tissues in animal models [5–7]. With such large scale ENM production potential in the near future, long-term exposures to ENMs in the workplace are likely to occur [8], however, minimal information is available for long-term exposures and the potential for ENM exposure-associated carcinogenesis.

Exposure to numerous occupational and urban air contaminants is suspected to initiate, via DNA damage, or promote tumorigenesis which alters cell signaling/crosstalk, expands damaged cells, and increases cancer hallmark behaviors, ultimately leading to neoplastic transformation and formation of an *in vivo* tumor [9]. Considering most ultrafine particles and ENMs deposit deep in the lung following inhalation [4], human primary small airway epithelial cells (pSAECs) represent one of the main targets following inspiration of ENMs and exhibit DNA damage, ROS, pro-inflammatory and cell damage signaling [10–12], which correlate to *in vivo* models of ENM exposure [13]. With hundreds of new ENM products in the market every year, evaluating numerous ENMs for carcinogenesis potential is quickly becoming a critical need for occupational risk assessment [14–15].

Few studies have focused on NMO carcinogenic potential. NMOs at nano and sub-micron ranges are released in various occupational settings with metal mass median concentrations between 0.73–1.47 $\mu g/m^3$, and even higher concentrations in personal breathing zones (3.3 – 47.67 $\mu g/m^3$) during handling activities [16,17]. One report describes silica-iron nanoparticle air concentrations up to 46,000 $\mu g/m^3$ inside a spray enclosure while outside spray enclosure concentrations were measured at 2.6 $\mu g/m^3$ [18]. Given the abilities of NMOs to penetrate, biopersist, damage, and initiate genotoxicity in exposed tissue, the possibility of ENM-induced or promoted tumorigenesis is a rising concern [14, 19–21].

Consistently, two NMOs with numerous nanotechnology applications, that have received increased toxicological testing attention, are nano-scaled cerium dioxide ($nCeO_2$) and ferric oxide (nFe_2O_3); thus, warranting further investigation into their carcinogenic potential. Cerium oxide, an oxidized lanthanide metal, is used in a variety of mechanical glass polishing applications, cosmetics as a UV absorber, and as a proficient catalyst as a diesel fuel additive to aid in emission reduction, which subsequently leads to its release in the particulate phase of exhaust [22,23]. While data is somewhat limited regarding the occupational exposure concentrations and limits, expected inhalation of $nCeO_2$ from diesel engines is estimated at approximately 0.09 $\mu g/kg$ body weight for 8 h [23]. Thus, total lung burden over human working life time would be approximately 936 $\mu g/kg$ [24]. Using a 10-fold safety factor, known rat mass, and lung surface area, 0.150 mg/kg – 7 mg/kg per rat or 0.008 $\mu g/cm^2$ – 0.35 $\mu g/cm^2$ alveolar surface area is a reasonable exposure range to assess pulmonary toxicity [24]. Cerium induces pneumoconiosis upon occupational exposure and is found in human alveoli and pulmonary interstitial tissue for decades post-exposure [22]. Mouse and rat *in vivo* studies reported pulmonary inflammation, lipid peroxidation, and fibrosis, as well as the bio-accumulation of $nCeO_2$ following exposure [21, 23, 24–28]. Although exposure route-dependent redox status discrepancies exist, $nCeO_2$ has also been shown to cause DNA damage and oxidative stress in human dermal fibroblasts and bronchial epithelial cells [27, 29, 30]. Past tumorigenesis studies in animal models suggest that micron-sized CeO_2 exhibits low tumorigenesis risk [31], however, little is known about $nCeO_2$ tumorigenesis risk and whether known inflammation, relatively low reactive oxygen species (ROS) generation, genotoxicity, and biopersistence contribute to tumor initiation and/or promotion.

Iron oxide nanoparticle (IONP) technologies have gained great interest and advancement due to its wide availability and its catalytic and paramagnetic properties suited for use in

biomedical imaging, paints, ceramics, catalysis, and pigments [32], however, concern over their use is warranted [33]. Current iron oxide fume fine particle occupational permissible and recommended exposure limit in ambient air over an 8 hour workday is 10 mg/m^3 (OSHA) and 5 mg/m^3, respectively (NIOSH). At present, no exposure limit for particle size (including nanometer) is proposed for iron oxide. Estimated tissue doses of airborne IONP in mice exposed to the current OSHA PEL is 0.003 – 2.2 μg/cm^2 in bronchioles and 0.003 – 0.13 μg/cm^2 in alveolar area [20]. Prolonged or high exposure to sub-micron and micron-sized particulates with bound iron, such as ambient particulate and asbestos, and combustion-derived iron oxide induces ROS, inflammation, and pneumoconiosis [34]. In addition, iron nanoparticle deposits are found in lung macrophages of welders and are thought to contribute to inflammation [35]. Iron is carcinogenic in animal models and prolonged elevated iron levels in tissue is widely believed to promote several human cancers, including lung cancer [36,37]. Recent iron nanoparticle *in vitro* epithelial and in *vivo* lung exposures show similar effects, with the addition of DNA fragmentation, inflammation-induced DNA adducts, hyperplasia, membrane damage, biopersistence and initial signs of fibrosis in exposed tissues [6, 20, 38, 39], although other studies show benign effects [reviewed by 33]. Given the large benefits of developing cerium and IONP technology and the perceived long-term health risks associated with exposure, establishing standardized *in vitro* assays to screen numerous ENMs for tumorigenic potential are urgently needed [15, 32].

The present work tested cell transformation potential of nCeO$_2$ and nFe$_2$O$_3$ compared to albumin-dispersed MWCNT, which served as a positive control particle. MWCNT were recently shown to initiate lung carcinogenesis in rats [40], promote tumor formation in mice [41], and cause neoplastic-like transformation [10]. In addition, herein we evaluated whether pSAECs could serve as a neoplastic transformation model, in addition to traditional immortalized cell models, to screen engineered nanomaterials for tumorigenesis risk. Such sub-chronic *in vitro* exposure models help identify complete carcinogens by capturing both initiation and promotion in early tumorigenesis [42]. We hypothesized that sub-chronic exposure to both nCeO$_2$ and nFe$_2$O$_3$ would cause early cell transformation and retention of neoplastic behavior in human pSAECs, similar to MWCNTs. Here, we show that continuous nFe$_2$O$_3$ exposure for 10 weeks caused immortalization and enhanced tumor-like phenotype in pSAECs, similar to MWCNT-exposed cells, while nCeO$_2$ exposure increased proliferation but did not cause immortalization or transformation. Collectively, our results demonstrate that prolonged nFe$_2$O$_3$ exposure harbors some tumorigenic potential that should be further explored. Additionally, this work suggests that human pSAECs can be used as a neoplastic transformation screening model for numerous ENMs for use in tiered risk assessment.

2. Methods

A more detailed description of Methods can be found in Appendix A.

2.1 Characterization of ENMs

$nCeO_2$ and nFe_2O_3 were manufactured in-house at Harvard University via flame spray pyrolysis using the Harvard Versatile Engineered Nanomaterial Generating System (VENGES) developed by the authors [43–45]. Specific surface area (SSA; m^2/g), was determined for powdered ENMs using nitrogen adsorption/Brunauer-Emmett-Teller method which was then used to calculate the BET equivalent primary particle size assuming spherical particles. MWCNT Mitsui #7 (Hodogaya Chemical) have previously undergone thorough characterization [46], and are known to promote lung adenocarcinoma and serosal lesions consistent with the diagnosis of sarcomatous mesothelioma *in vivo* [41]. All materials were characterized using x-ray diffraction diameter, density, and FESEM [25, 43–45].

2.2 ENM Dispersal, Characterization in Suspension, and Dosimetric Considerations for In Vitro Testing

Stock solutions of NMOs (0.1 mg/ml) were prepared by dilution of 1 mg/ml stock solutions with sterile MilliQ water. NMO solutions were sonicated in water, while 0.1 mg/ml MWCNT solutions (1 mg/ml) were sonicated in 1.5% v/v bovine serum albumin (BSA) dispersant solution using a SonicCell cup sonicator to achieve uniform dispersion [47]. Each dispersed ENM was serially diluted with small airway epithelial cell growth medium (SAGM) to the reported concentrations and characterized for intensity-weighted hydrodynamic diameter (dH), polydispersity index (PdI), zeta potential (ζ), and specific conductance (σ) by dynamic light scattering (DLS) following established protocols [48]. The recently developed Volumetric Centrifugation Method (VCM) [49] determined to measure effective density (ρ_{agg}) of the formed agglomerates. Advanced distorted grid (DG) fate and transport modeling was conducted to report Relevant *In Vitro* Dosimetry functions as described in Appendix A following published procedures [47, 50, 51].

2.3 ENM Uptake and Cellular Localization

Uptake and localization analysis of ENM in pSAECs (Lonza) was performed using enhanced darkfield imaging following a 24 h exposure, as previously described [10]. Briefly, pSAECs were seeded onto conditioned coverslips in a 24-well plate, and exposed in duplicate to administered doses of either dispersed 0.06 $\mu g/cm^2$ NMO or 0.06 $\mu g/cm^2$ MWCNTs for 24 h. Fixed and stained cells were imaged with an Olympus microscope equipped with Cytoviva. Next, ENM intracellular localization was assessed via transmission electron microscopy (TEM; JEOL 1220, Tokyo) following exposure to all ENMs (0.6 $\mu g/cm^2$) for 24 h using previously described methods [13,24].

2.4 Sub-chronic exposure to primary SAEC

Human pSAEC (Lonza) were seeded in a 25 cm^2 flask holding small airway basal medium supplemented with Clonetics Growth Supplements (Lonza) and 1% penicillin/streptomycin to obtain small airway growth medium (SAGM). Cells were cultured in a humid atmosphere at 37°C containing 5% CO_2 air with medium changes every 3 days, per manufacturer's instructions. For passaging, all cell cultures were washed in HEPES-buffered saline, incubated in one volume of 0.25% Trypsin/EDTA for 5 m, and neutralized in 2 volumes of

trypsin neutralization saline following manufacturer's protocol (Lonza). Unexposed, low passage immortalized SAECs (hTERT) were cultured in identical conditions and periodically used as a comparative control.

To initiate exposure, pSAECs were seeded (5×10^4/well) overnight in triplicate to tissue culture treated 6-well plates (BD Falcon). Following seeding, cells were continuously exposed to administered doses of 0.6 μg/cm^2 dispersed nCeO$_2$, or nFe$_2$O$_3$, or 0.06 μg/cm^2 MWCNT twice a week for up to 12 weeks, as previously described with modifications [10]. Briefly, NMO administered doses were based on estimated worst case exposure scenarios and/or documented upper limit exposure levels. The nCeO$_2$ dose, calculated by deposited mass per rat lung surface area, reflected a worst-case exposure (~10 mg/kg) over a working lifetime exposure to nCeO$_2$-containing diesel exhaust and was shown to induce inflammation, lung damage, and onset of lung fibrosis in exposed rat lung [24]. Likewise, the nFe$_2$O$_3$ dose (0.6 μg/cm^2) represents deposited dosimetry for IONPs at the current OSHA permissible exposure limit (PEL) [20]. The MWCNT dose reflected a reasonable occupational exposure with an expected deposited dose in a 30 μg/mouse model, known to cause chromosome aneuploidy, mirrored a CNT lung burden known to promote lung cancer, and results in neoplastic-like transformation in human SAECs [10,41]. Cells were rinsed once in ENM-free warm growth medium and re-exposed every three days, and passaged every ~6 – 9 days throughout the experiment. Exposed cells were passage matched to saline and dispersant-only cells throughout experiment.

2.5 Cancer Hallmark Assessment

Sub-chronic exposed cells were assayed at 6 and 10 weeks of exposure duration for several cancer cell hallmark behaviors including WST-1 cell proliferation, Transwell invasion, soft agar colony formation, and morphological transformation using previously described standardized methods with minor modifications [10]. More detail can be found in Appendix A.

2.7 Clonal Expansion and Cancer Hallmark Assessment

To further evaluate neoplastic transformation in ENM-exposed pSAECs, 10 to 12 soft agar colonies were removed from 10 week exposed treatments, and re-established in culture for cancer hallmark evaluation as described above and in Appendix A. Briefly, a small core of agar containing each colony was removed from suspension, transferred to 48-well plates, cultured in SAGM, and expanded in 6-well plates to acquire colony clones for hallmark screening and protein expression analyses.

nFe$_2$O$_3$ and MWCNT clones were evaluated for retention of the enhanced cell proliferation, invasion, and soft agar colony formation, as previously described, compared to saline-, albumin-, and 10 week-exposed cells. Saline and albumin-exposed cells were used for both proliferation and invasion assays. In addition, apoptosis resistance via either the intrinsic or extrinsic pathway was evaluated by conducting dose-response studies using tumor necrosis factor alpha (TNF-α) and FAS ligand (FasL). Since saline and albumin-treated cells underwent senescence after 12 weeks in culture, low passage pSAECs were used as appropriate negative controls for a normal epithelial cell phenotype in the apoptotic

resistance assay. Briefly, cells exposed to nFe_2O_3 for 10 weeks, nFe_2O_3 clones, and MWCNT clones (1×10^4) exposed to 0 – 50 ng/ml TNF-α, 0 – 30 μM antimycin-α, and 0 – 50 ng/ml FasL for 24 h according to previously described methods [52]. Next, cells were stained with a Hoescht 33342 and propidium iodide (PI) fluorescent dye cocktail, imaged with the ImageXpress Micro XLS system (IMX; Molecular Devices, LLC) to quantitatively score live, apoptotic and necrotic cells. Data were exported to Excel for further statistical analysis.

2.8 Live cell and ROS generation quantification following acute exposure

pSAECs (5×10^3) were seeded into each well of a 96-well plate overnight and then exposed to administered doses ranging 0 – 2 μg/cm^2 of each NMO for 24 and 48 h in sextuplet. Live and dead cells were stained with 1 μM Hoescht 33342 and 10 μg/ml PI and imaged at 4X magnification on the IMX system. To determine ROS generation potential of NMO exposure, cells (5×10^3) were plated in triplicate in a 96-well plate and exposed to each NMO and MWCNT for 1 – 48 h. Following exposure, cells were stained with either MitoSox Red (Molecular Probes) or $2',7'$-dichlorofluorescin diacetate (DCF; Sigma Aldrich), and Hoescht 33342 (Invitrogen) for 30 minutes, washed twice with fresh medium, and subsequently imaged at 10X magnification with the IMX system. MitoSox Red and DCF stain intensity was determined and exported as previously described above.

2.9 Western Blot analysis of key proteins for iron homeostasis

SAEC-hTERTs (5×10^5 cells) were plated in the wells of a 6-well plate overnight then exposed to an ENM particle-containing medium for 24 or 48 h. Sub-chronic exposed cells and low passage pSAECs were plated at the same density and cultured for either 24 or 48 h. Protein was isolated from all cells following previously described methods [10]. Equal mass of isolated protein were separated by 10% bis-Tris acrylamide gels and transferred to nitrocellulose membranes. Membranes were probed with primary CD71, FTH1, GAPDH (Cell Signaling) and SCL40A1 (Abcam) DMT1 (Abcam) antibodies, incubated with secondary anti-rabbit or anti-mouse (Santa Cruz Biotechnology) HRP-conjugated antibody, and incubated in chemiluminescent substrate for X-ray film detection. Densitometry was performed on protein bands using ImageJ software (NIH).

2.10 Intracellular iron assessment

SAEC-hTERTs (2×10^6) were plated in triplicate to 10 cm^2 culture plates and exposed to administered doses of either 0, 0.06, or 0.6 μg/cm^2 of each ENM for 48 h. SAEC-hTERT were used since obtaining enough low passage pSAEC to assess iron levels was not feasible. Following exposure, intracellular iron was assessed using the Iron Assay kit according to the manufacturer's instructions (Sigma Aldrich). Low passage, unexposed pSAECs and sub-chronic-exposed pSAECs were also assessed for iron content. Samples with equal mass ENM without cells were used as particle controls. Briefly, supernatants from lysed cells were split in half to two aliquots, diluted 1:1 v/v with assay buffer, and added in triplicate to a 96-well plate. Iron reducing reagent was added to one aliquot while equal volume of buffer was added to the other aliquot to determine total and ferrous iron (Fe^{2+}), respectively. Lastly, samples were incubated with an iron probe and absorbance assayed at 593 nm. Absorbance

values were corrected from background and PBS buffer controls, then normalized for live cell count (2×10^6) due to ENM toxicity at 6 μg/cm^2 in some treatments.

2.11 Statistical Analysis

All datasets were imported into SAS JMP v.10 and analyzed for normal distribution of residuals and variance homogeneity using goodness of fit tests and Bartlett's test. Data were log-transformed to achieve normal distributions. Treatments were compared using one- or two-way ANOVA followed by Dunnett's or Tukey-Kramer HSD post-hoc tests (α = 0.05). For those data lacking equal variance, the Kruskal-Wallis test using χ^2 statistic was used to compare treatments.

3. Results

3.1 Characterization of ENMs

Table 1 summarizes the characterization of the dry ENM powders used in the study, including specific surface area and primary particle diameters. $nCeO_2$ was previously described as loose agglomerates with fractal structure following VENGES synthesis as determined by TEM [25]. Similarly, nFe_2O_3 [45] existed as aggregates/agglomerates with smaller primary particles. $nCeO_2$ primary particle crystal size was 2-fold larger (d_{XRD}) than nFe_2O_3. MWCNTs, previously characterized [46], possessed typical high-aspect ratio fiber characteristics. nFe_2O_3 primary particles possessed greater surface area (96 m^2/g) than $nCeO_2$ (59 m^2/g) and MWCNTs (26 m^2/g).

Table 2 describes the properties of the tested ENMs suspended in SAGM. Although $nCeO_2$ exhibited 10-fold larger agglomerate d_H than nFe_2O_3 in water, $nCeO_2$ and nFe_2O_3 had a similar volume-weighted d_H of 341 nm in SAGM, and displayed a polydispersity index (PdI) of 0.401 ($nCeO_2$) and 0.271 (nFe_2O_3), which is representative of a fairly monodispersed suspension. Comparable zeta potential and conductivity measurements were also observed in the NMO suspensions of approximately −11 mV and conductivities ranging from 8.76 to 11.10 mS/cm. nFe_2O_3 and MWCNTs exhibited strong positive surface charge in water, which switched to minimal negative charge in SAGM medium. $nCeO_2$ showed minimal change between water or media suspensions.

3.2 Dosimetric Considerations For In Vitro Testing

The delivered cell dose at a given exposure time point may not always be the same as the dose administered [47] due to the differential settling rate of the formed agglomerates *in vitro.* This is defined by two fundamental parameters, the hydrodynamic diameter, d_H, of the formed agglomerate and its effective density, ρ_{agg} [47,49]. Using the recently developed Harvard *in vitro* dosimetry methodology [47, 51], the fraction of the administered particles that deposit on the cells located at the bottom of the treatment well as a function of time was calculated (Figure 1A). The deposition fraction constants (α_1 and α_2) as well as the RID functions for both NMO particle suspensions are presented (Table 3) for both of the experimental conditions used in the study. The $nCeO_2$ and nFe_2O_3 deposited at a similar rate, with an approximate fraction deposited of 0.3 when suspended in SAGM for 48–72 hours for the sub-chronic (left panel) and acute (right panel) exposure studies. Thus, both

administered dose and deposited dose were calculated and reported for the remainder of the study.

3.3 NMO uptake

Exposure of $nCeO_2$ or nFe_2O_3 for 48 h resulted in co-localization of each NMO within pSAEC cytoplasm (Figure 1B) with occasional perinuclear localization (Figure B.1). Minimal nuclear co-localization of the NMOs was observed. To further assess NMO cellular fate in exposed cells, TEM analysis following 24 h exposure revealed evidence for pSAEC ENM phagocytosis (Figure 1C–E). Podia-like projections were observed surrounding loose agglomerates of both $nCeO_2$ and nFe_2O_3 (Figure 1C). Close examination of the cell periphery and cytoplasm found that $nCeO_2$ was present both in membrane-enclosed vesicles and free suspension in cytoplasm. Loose agglomerates of nFe_2O_3 were exclusively found in membrane-bound vesicles (Figure 1D and E). Using enhanced darkfield imaging, MWCNTs co-localized with the plasma membrane, cytoplasm, and nucleus (Figure B.1A) of the pSAECs. Fine focus adjustment during imaging suggested that MWCNTs had punctured both cell and nuclear membranes. In TEM analysis, MWCNTs were observed undergoing phagocytosis, piercing cell plasma membranes, or piercing membrane-bound vesicle (Figure B.2).

3.4 Cancer Hallmark Assessment

During sub-chronic exposure, all exposed pSAECs were observed to occasionally change shape, following trypsinization, passaging, and reseeding, from a cuboidal appearance to a more fibroblast-like appearance. As cultures reached greater than 60–70% confluence, pSAECs would take on a more cuboidal shape, thus suggesting pSAECs were undergoing transient wound healing response under epithelial-mesenchymal transition (EMT) and mesenchymal-epithelial transition (MET) cell signaling [53]. Following continuous 6 and 10 week exposures, sub-confluent NMO- or MWCNT-exposed pSAECs possessed an altered cell morphology characterized by a more rounded cell body with some podia (Figure 2A). This contrasted with both saline (NMO vehicle) and albumin dispersant (MWCNT vehicle) passaged cells that possessed a more elongated cell body under sub-confluent conditions. No gross abnormal nuclei (i.e. bi-or multinuclear) cell bodies were observed.

Following 6 weeks of exposure, $nCeO_2$- and MWCNT-exposed cells exhibited significantly greater cell proliferation ability, 1.3- to 1.6-fold increase, than saline and albumin passage controls (Figure 2B, p   0.05), as assessed by WST-1 assay. Conversely, nFe_2O_3-exposed cells experienced significant reduction (~40%) in proliferation compared to saline controls (p<0.05). All cell types did not show a difference between 24 and 48 h time point possibly due to low proliferation rate and attachment-associated behaviors post-seeding.

At 10 week exposure, cells were assayed at 48 and 72 h post-exposure to better assess proliferation ability of the culture. Exposure of pSAECs to different NMOs affected cell proliferation in a time dependent manner (Figure 2C, p   0.05). Specifically, $nCeO_2$ and nFe_2O_3 cells experienced significant 4- to 13-fold increases in cell proliferation at 48 h, respectively, compared to saline passage control cells. nFe_2O_3 cell proliferation at 72 h was significantly greater than $nCeO_2$ cells. In contrast, MWCNT-exposed cells exhibited a

significant, but minimal (1.1-fold, p   0.05), increase in cell proliferation compared to albumin-only passage controls, while albumin passaged cells possessed significant enhanced proliferation compared to saline passage control. Following an 8-day recovery post-exposure, 10 week saline passage control cells showed a significant 5-fold reduction in proliferation compared to 6 week saline control cells, suggesting that 10 week cells started to exhibit pre-senescent growth (Figure 2D). This was confirmed one week later with cessation of cell growth in 11 week old saline control cultures (data not shown). In the absence of NMO particles, 10 week old pSAECs displayed a 2- to 2.5-fold reduction in proliferation ability at 48 h, but remained significantly higher than saline passaged controls. Conversely, MWCNT exposed pSAECs exhibited a striking significant reduction in proliferation ability compared to albumin passage control cells (Figure 2D; p   0.05). Similar to saline passage control cells, albumin-only and $nCeO_2$ exposed cells experienced senescence at 11 – 12 weeks in culture (1–2 weeks post-10 week exposure; data not shown). Conversely, 10 week-exposed nFe_2O_3 cells remained viable and retained proliferation ability well past 12 weeks in culture. In summary, these results indicated that $nCeO_2$ and MWCNT exposure caused transient cell hyperplasia in pSAEC. In addition, the proliferative effects of nFe_2O_3 exposure were better retained in recovery than MWCNT-exposed cells.

To assess potential aggressive behavior in NMO- and MWCNT-exposed pSAECs, cells were evaluated for chemotactic invasion ability in Matrigel coated transwell inserts. Since 10 week old primary cultures exhibited signs of pre-senescence, SAEC-hTERTs were used as an additional comparative control. Both SAEC-hTERT and $nCeO_2$-exposed pSAECs possessed significant enhanced invasion ability compared to saline passage control (Figure B.3, p   0.05). Strikingly, nFe_2O_3 cells exhibited a significant 21-fold and 3.7-fold increase in invasion ability compared to saline and $nCeO_2$-exposed cells, respectively (p   0.05). MWCNT-exposed cells exhibited a minimal but significant increase in invasion compared to albumin control (p   0.05).

The ability of exposed pSAECs to undergo attachment-independent growth and colony formation was assessed using soft agar colony formation assay. At 6 weeks, only 12 and 17 colonies total were found in nFe_2O_3 and MWCNT plates, respectively (Figure 3A and B). At 10 weeks, all ENM-exposed cells exhibited significant increases in colony formation compared to 6 week cells, saline, and albumin passage controls. nFe_2O_3- and MWCNT-exposed cells exhibited a 11- and 5-fold significant enhanced colony formation ability compared to $nCeO_2$ cells, respectively (Figure 3B). No colonies were found in saline or albumin passage controls at either time point.

Morphological transformation assessment typically relies on two assays, colony forming efficiency (cytotoxicity) and cell transformation (invasive Type III foci on a confluent monolayer), with malignantly transformed cells showing elevated levels in both assays [54,55]. Our data found that attached colony formation ability was dependent on the type of ENM particle and exposure time (Figure 3C, p   0.05). nFe_2O_3- and MWCNT-exposed pSAECs exhibited similar significant increased colony formation ability following 6 and 10 week exposure (p   0.05). Surprisingly, $nCeO_2$-exposed cells after 6 and 10 week exposure failed to form viable proliferating colonies, possibly due to low survival ability at low seeding density and absence of $nCeO_2$ particle stimulatory effect. Saline and albumin

control cells showed minimal or no survival ability at low density seeding at either time point.

At 6 weeks, nFe_2O_3- and MWCNT-exposed pSAECs exhibited weak to moderate morphological transformation qualitative phenotypes. Each cell type exhibited numerous Type I foci in confluent plates with the presence of cells containing abnormal nuclear morphology (Figure 3D). Only cells exposed to nFe_2O_3 developed several Type II foci, with surrounding bi-nucleated cells observed (Figure 3D). In MWCNT-exposed cells, large polynucleated 'giant cells' ranging from 150 – 500 μm in diameter were observed (Figure 3D and Figure B.4). At 10 weeks, only occasional Type I foci were found in nFe_2O_3 and MWCNT cells with rare occurrence of Type II foci in MWCNT-exposed cells only. $nCeO_2$ exhibited confluent single cell layers and minimal evidence for morphological transformation following 6 week and 10 week exposures.

At two weeks post-10 week exposure, both nFe_2O_3- and MWCNT-exposed pSAECs exhibited retention of enhanced cell proliferation ability compared to controls. At 18 days post-exposure (3rd passage post-exposure), one subset of cells were kept in culture while aliquots were frozen in liquid nitrogen following the manufacturer's freezing protocol to assess acquisition of immortality. Both fresh and frozen 10 week nFe_2O_3-exposed cells retained proliferation ability for further culturing and were assayed for the remainder of the study. Unfrozen nFe_2O_3 cells were cultured out to 30 passages with no stoppage in proliferative culture capacity. Conversely, both fresh and frozen MWCNT-exposed cells only survived until 5th and 6th passage post-exposure, respectively, until senescence (data not shown), possibly due to the absence of MWCNT particle stimulatory effect (Figure 2) and its known ability to damage DNA. 10 week-exposed MWCNT cells were used in clonal cell proliferation experiments (described below) prior to senescence. These observations suggest that 10 week nFe_2O_3 exposure to pSAEC resulted in an immortalization-like effect while MWCNT exposure did not result in an immortalization effect.

3.5 Colony clone neoplastic behavior

Based on the short life span of pSAEC in culture, and evidence for nFe_2O_3 and MWCNT cell transformation, we isolated and expanded clones from soft agar colonies from each of these treatments to further assess transient or persistent cancer cell hallmark phenotypes in these transformed cells. Reestablished clones from 10 week-exposed nFe_2O_3 and MWCNT cells experienced >80% survival through the clonal expansion procedure (Figure B.5). Surprisingly, $nCeO_2$ colonies placed back into culture arrested growth and underwent cell death within 2 weeks of colony collection. No attached $nCeO_2$ colony clones were observed on bottom of the well. Furthermore, confluent cultures of nFe_2O_3 and MWCNT clones, at 2 passages post-clonal establishment, exhibited foci formation indicating escape from contact inhibition signaling and were consistent with Type II foci (Figure 4A and B). Sub-confluent nFe_2O_3 and MWCNT cells exhibited a squamous morphology, while a few cells were observed to possess binuclear or polynuclear morphology which was never observed in either unexposed or 10 week original pSAEC cultures. Cells were re-evaluated at 4 passages post-clonal isolation resulting in no bi- or poly-nucleated cells were observed (data not shown).

Evaluation of cell proliferation ability revealed that both nFe_2O_3 and MWCNT colony clones exhibited retention of enhanced proliferation compared to 10 week old saline and albumin passage controls (Figure 4C). nFe_2O_3 clones exhibited a significant reduction in proliferation ability compared to 10 week immortalized nFe_2O_3 cells. Interestingly, MWCNT clones exhibited equivalent proliferation ability to MWCNT 10 week exposed cells. Following nFe_2O_3 and MWCNT clone proliferation ability, 8 different clones from each particle treatment were aliquoted and frozen to evaluate freeze survival ability and immortalization. All frozen clones were successful in re-establishing culture and proliferation ability following freezing (data not shown). Non-frozen clones were used for all subsequent cancer cell hallmark assessments in this study.

Reassessment of soft agar colony forming ability in clones found that nFe_2O_3 clones exhibited significant enhanced (~2.5-fold) soft agar colony forming ability compared to 10 week-exposed cells (Figure 4D), while MWCNT clones exhibited a minimal, yet significant, increase in colony forming ability compared to 10 week cells. Conversely, both nFe_2O_3 and MWCNT clones showed significant reduction (~3-fold) in invasion ability compared to their 10 week-exposed counterparts (Figure 4E), but still were significantly above both saline and albumin passage controls.

Next, we assessed 10 week-exposed nFe_2O_3 cells, nFe_2O_3 clones, and MWCNT clones resistance to extrinsic and intrinsic apoptosis signaling. Low passage pSAEC exhibited 60% viability while nFe_2O_3 10 week, nFe_2O_3 clones, and MWCNT clones exhibited >90% viability (Figure 4F) without FasL treatment. All cells exhibited a significant, dose-dependent decrease in viability upon FasL exposure (5 and 50 ng/ml), but ENM-exposed cells exhibited a significant increase in viability compared to low passage pSAECs at each FasL dose. In addition, 10 week nFe_2O_3 cells and nFe_2O_3 clones exhibited significant elevation in viability at 50 ng/ml FasL compared to MWCNT clones. These trends indicated that ENM exposure caused a basal apoptotic resistance ability in the extrinsic pathway compared to parent pSAECs, and that nFe_2O_3-exposed cells exhibited greater resistance than MWCNT clones at high dose. Exposure to TNF-α (0 – 50 ng/ml) or antimycin-a (0–30 μM) to all cell types resulted in 15–20% increase in apoptosis with no significant difference between treatment groups ($p > 0.05$; data not shown).

3.6 Superoxide radical and ROS generation

Next, nFe_2O_3 and MWCNT clones were evaluated for potential mechanisms promoting pSAEC neoplastic-like transformation and immortalization characteristics. Since ENM exposure can result in ROS generation and insoluble particles contribute to disruption of iron homeostasis and elevated ROS [34], we conducted acute exposures of both NMOs and MWCNTs to pSAECs and SAEC-hTERTs to evaluate these potential effects. $nCeO_2$, nFe_2O_3, and MWCNT exposure (1.8 – 60 ng/cm^2 delivered) elicited significant increase in superoxide radical generation ability at 1 h compared to saline-only exposed controls (Figure 5A, Figure B.6). Similarly, nFe_2O_3 and MWCNT exposure caused an increase in intracellular ROS species at 24 h (Figure 5B and Figure B.7; p 0.05). Alternatively, increasing doses of $nCeO_2$ caused significant reduction of intracellular ROS to pSAEC basal levels, suggesting anti-oxidant potential (i.e. 0.168 $μg/cm^2$). Since moderate or high ROS

generation can stimulate cell proliferation or cell death pathways, we evaluated acute cell proliferation ability. Acute nFe_2O_3 exposure resulted in significantly elevated cell proliferation between 0.006 – 0.177 μg/cm^2 delivered, while $nCeO_2$ exposure had no effect (Figure B.8). Taken together, moderate exposure to nFe_2O_3 results in ROS generation and stimulation of cell proliferation.

3.7 Iron Assay

To identify potential changes in intracellular iron content which may drive ROS generation via the Fenton reaction, SAEC-hTERTs were exposed to 0.018 and 0.18 μg/cm^2 delivered of each ENM for 48 hours and assayed for intracellular iron. Exposure to nFe_2O_3 caused a significant increase in Fe^{2+} in lysed cell supernatant (Figure 5C, F=10.4, p = 0.011), while $nCeO_2$ and MWCNT exhibited minimal change compared to unexposed cells (p > 0.05). No statistical difference in Fe^{2+} concentration existed between 0.06 and 0.6 μg/cm^2 nFe_2O_3-exposed cells. Intracellular soluble ferric iron (Fe^{3+}) levels were negligible across all treatments with no significant changes observed compared to the unexposed control (p > 0.05; data not shown).

3.8 Iron transport protein expression analysis

Based on the observed enhanced ROS generation and intracellular iron content, we next assessed several key proteins associated with uptake (transferrin receptor, CD71; divalent metal ion transporter, DMT1), storage (ferritin, FTH1), and export of soluble iron (ferriportin, SLC40A1) in lung epithelial cells following acute and sub-chronic exposure to NMOs and MWCNTs [34,37]. Alterations to these proteins can impact loosely bound iron in the cytoplasm (i.e. labile iron pool), thus influencing redox reactions and ROS generation. Following acute 24 h exposure of each NMO to SAEC-hTERTs, CD71 displayed a significant 4-fold increase in expression at 0.0018 – 0.06 μg/cm^2 delivered (Figure 5D), while higher doses caused no significant effect. Alternatively, DMT1 expression level did not significantly change under $nCeO_2$ exposure, while moderate nFe_2O_3 doses resulted in significant elevation compared to unexposed cells (all χ^2 = 7.4; p 0.05). Acute exposure to ENMs (0 – 0.18 μg/cm^2 delivered) resulted in no significant change in FTH1 expression (Figure B.9). SLC40A1 exhibited relatively low expression level that did not significantly change following NMO exposure (all χ^2 < 6.4, p > 0.05). These data suggested that NMO-exposed SAEC-hTERTs experienced increased uptake of iron during acute exposure.

Lastly, we assessed prolonged changes in iron transport and storage ability in Fe_2O_3 and MWCNT transformed pSAECs. nFe_2O_3-transformed and nFe_2O_3 clones displayed a significant decrease in CD71 expression, while MWCNT clones displayed no significant change compared to low passage unexposed pSAECs (Figure 6A and D). Alternatively, transformed cells and clones exhibited a significant increase in DMT1 (Figure 6B and D). nFe_2O_3 cells possessed a 3.1-fold increase compared to control. Both nFe_2O_3 and MWCNT clones, however, exhibited a 14 to 17-fold increase compared to nFe_2O_3-transformed cells suggesting that over-expression of DMT1 is associated with a colony formation phenotype. Next, nFe_2O_3-transformed cells and clones displayed a significant 2-fold reduction in FTH1 expression while no significant effect was observed in MWCNT clones compared to unexposed pSAECs (Figure 6C and D). Lastly, MWCNT clones displayed a significant 4-

fold decrease in SLC40A1 expression while all other cell types did not differ from unexposed pSAECs.

To ascertain whether transformed Fe_2O_3- and MWCNT-exposed pSAECs exhibited enhanced ability to store intracellular iron, each sub-chronic cell type and isolated clones were assayed for intracellular iron compared to low passage, unexposed primary SAECs. Both transformed Fe_2O_3 and MWCNT-exposed cells possessed significantly elevated (2- to 4-fold) Fe^{2+} content compared to controls and respective clones (Figure 6E; p ≤ 0.05). nFe_2O_3 and MWCNT clones exhibited a reduced, but still significantly elevated, levels of intracellular Fe^{2+} compared to controls. In addition, 11.4% of total intracellular iron in Fe_2O_3-transformed cells was Fe^{3+}, which was not observed in any other acute or sub-chronic exposed treatment group. Coupled with iron transport and storage protein expression data, these data suggested that sub-chronic exposure to ENMs with cell transformation ability results in increased ability to move divalent metal ions across cell membranes and lowered intracellular iron storage capacity in favor of an increased intracellular labile iron pool.

4. Discussion

Given that low concentration, chronic exposures are predicted from increased ENM production and use across their lifecycle), very few studies have evaluated ENMs for carcinogenic potential and no standardized testing framework exists, even as ENMs are quickly entering mass production and wide distribution [8,14, 56]. The current study evaluated the neoplastic transformation potential of two widely used NMOs, $nCeO_2$ and nFe_2O_3, compared to an established ENM tumor promoter, MWCNT, in a human pSAEC model. To our knowledge, this study is the first to screen NMOs as complete carcinogens evidenced by neoplastic transformation potential following occupationally relevant exposure (0.18 μg/cm^2) in a human lung epithelial cell model. Special emphasis was given to take into consideration the delivered doses to cells rather than the administered doses to be able to more accurately rank bioactivities across the various ENMs. We concluded that sub-chronic exposure to nFe_2O_3 for 10 weeks at a delivered dose of 0.180 μg/cm^2 resulted in a neoplastic-like transformation and replicative immortalization of human pSAECs, similar to MWCNT, suggesting that occupational nFe_2O_3 exposure harbors risk for early neoplastic-like transformation in the human lung.

Our continuous exposure method of treating cells every three days resulted in exposed pSAECs receiving 30–31% of the 0.6 μg/cm^2 administered dose for both NMOs tested. Conversely, it is estimated that >90% of 0.06 μg/cm^2 of MWCNT dispersed in albumin was delivered to exposed cells, based on their high aspect ratio, density, and hydrophobicity [57]. For simplicity we assumed that 100% of MWCNTs was delivered and that delivered and administered doses for MWCNTs was identical. Settling rates and eventual deposition of low aspect ratio nanoparticles onto attached *in vitro* cell models are determined by agglomerate size, effective density, sedimentation, diffusion, particle solubilization, and boundary layer absorption [47,49]. Both dispersed NMOs in SAGM medium exhibited similar hydrologic diameters and effective densities resulting in similar DG-modeled delivered mass, particle number, and surface area doses. Considering >90% of the 0.3

deposited NMO fractions occurred within the first 6–8 h for 6-well plates and 18–22 h in 96-well plates, respectively, it appears that sedimentation onto the reflective boundary layer on the well bottom resulted in an upward diffusion gradient, then an equilibrium, thus minimizing further NMO deposition [49]. Since both NMOs exhibited similar delivered doses, the observed differences in pSAEC behavior and transformation can be attributed to their inherent physicochemical properties.

$nCeO_2$ displayed enhanced proliferation ability, however, showed little evidence of aggressive neoplastic behavior. CeO_2 valence states may contribute to cell proliferation (Ce^{4+}) or inhibition (Ce^{3+}) [58], in part due to its intra- and extracellular ROS sequestration ability [59]. In addition, a particle's cellular fate and peroxide radical cycling ability may determine ROS-associated impacts on growth, survival, and disease development [28, 29, 60, 61]. Here, increasing doses of nCeO2 reduced ROS levels thus suggesting $nCeO_2$ acted as an anti-oxidant during the sub-chronic exposure. Several studies support our findings of ceria not promoting invasion or colony formation ability in malignant cells. Rather, it may act as an anti-cancer therapeutic [30] since it reduced promotion effects of known initiators and subsequent BALB/3T3 cell transformation *in vitro* [62]. Less reactive particles with moderate ROS generation or sequestration ability (e.g. ultrafine carbon black) typically show increased proliferation with low to moderate *in vitro* cell transformation ability compared to more reactive materials [10]. Past research studies showed that pulmonary exposure to cerium oxide resulted in no significant development of lung tumorigenesis. Single inhalation exposure to CeO_2 resulted in 7 out of 1049 rats developing alveolar papillary neoplasms, adenocarcinoma, or carcinoma across their lifespan [31] that compared to unexposed animals. Given conflicting reports of the ability of ceria nanoparticles to generate ROS and cause DNA damage, the likelihood for potential neoplastic transformation may depend on particle fate, biopersistence, valence state, and persistent inflammation in exposed tissues.

Since the immortalized nFe_2O_3-transformed cells, nFe_2O_3 clones, MWCNT-transformed cells, and MWCNT clones showed increased survival ability (Figure 3C), moderate morphological transformation (Figure 3D), enhanced proliferation (Figure 4C), and acquisition/retention of soft agar colony forming ability (Figures 3B and 4D), the transformation can be interpreted as an early neoplastic phenotype [9, 63], since occasional Type II foci does not typify a malignant transformed cell [63]. MWCNTs (Mitsui #7) have a well-documented toxicological history in that they exhibit deep interstitial penetration, biopersistence, extrapulmonary transport, and promotion of lung adenocarcinoma and pleural mesothelioma [5, 41, 46] while *in vitro* studies with human SAECs (0.02 – 2.4 $\mu g/cm^2$) reported aneuploidy and neoplastic-like transformation [10, 11]. To date, most IONP *in vitro* toxicity studies have conducted acute, high dose exposures to evaluate genotoxicity, ROS production, proliferation, and cytotoxicity to model biomedical or dermal exposures [33, 64], including conflicting IONP cell transformation effects at high doses [65, 66]. Collectively, nFe_2O_3 reportedly displayed a less potent effects than other IONPs [67,68]. Few studies have evaluated prolonged, low dose exposures to NMOs that possess high surface area, suspected genotoxic, and ROS-generating abilities, all known factors in tumorigenic initiation and promotion and are known effects following exposure to a complete carcinogen. Here, continuous exposure potentially caused prolonged ROS

generation resulting in accumulation of oxidative damage thus affecting cell proliferation and survival (i.e. 6 week data). The large gain and retention of proliferation rate well into post-exposure suggest that cells had switched from a damaged cell phenotype attempting to control ROS stress to a hyperplastic phenotype that potentially relied on particle-associated ROS generation. Numerous studies examining the effects of other soluble and micron-sized metals report similar phenomenon. Human bronchial epithelial cells were shown to switch from slowed, stressed phenotype to one that was highly proliferative and dependent on ROS signaling that promoted several cancer cell hallmarks [69].

At present conflicting reports on nFe_2O_3 toxicity following inhalation exposure exist on whether nFe_2O_3 exposure harbors significant pulmonary health risk. Sub-micron and micron-scaled Fe_2O_3 found in mild steel welding fumes typically does not result in lung tumorigenesis in chronically exposed welders [70], although this finding has been challenged [71]. Comparisons of pulmonary toxicity between nano-sized FeO, Fe_2O_3, and Fe_3O_4 found that nFe_2O_3 is relatively non-bioavailable (i.e. low free Fe ions) resulting in low toxicity compared to FeO and Fe_3O_4 [67]. Other recent *in vivo* reports suggest that respirable nFe_2O_3 caused alveolar wall damage, interstitium biopersistence, ROS-induced damage, inflammation, hemosiderin deposits, hyperplasia, and signs of fibrosis [6, 72, 73], with notable increased liver iron concentrations, inflammation, hyperemia, and hyperplasia. VENGES-generated nFe_2O_3 particles were shown to induce pulmonary tissue damage and inflammation following intratracheal (i.t.) exposure in rats [43], and elicited ROS generation in heart tissue following inhalation at $100–200 \mu g/m^3$ [44]. Given these reports of adverse outcomes commonly associated with early neoplasm development that align with this study's findings, further research into nFe_2O_3 long-term pulmonary exposure to identify potential tumorigenic risk is needed.

Immortalization and neoplastic-like transformation of sub-chronic nFe_2O_3-exposed cells suggests disruption of iron homeostasis in the form of elevated labile ferrous iron pool, ROS generation, and elevated oxidative damage. Iron serves several critical roles in mammalian cells, however, excessive accumulation of iron in tissue is associated with numerous chronic pathologies, including cancer [34, 37, 74]. In biological systems, iron exists as Fe^{2+} or Fe^{3+} through gain or loss of electrons allowing for catalysis of oxygen species through the Fenton and Harbor-Weiss reactions leading to generation of ROS [34]. Thus, mammalian tissues are highly adapted to uptake, store, metabolize, and eliminate soluble and insoluble iron based on balancing physiological needs and toxicity resulting in iron homeostasis. Persistent iron overload or depletion is associated with numerous clinical pathologies including increased infection, cancer, anemia, and liver cirrhosis [34,37]. Here, nFe_2O_3 uptake into SAEC phagocytic vesicles and increased intracellular Fe^{2+} suggested that these particles experienced solubilization in acidic phagolysosomes and eventual release of Fe^{2+} into the cytoplasm to enter the cellular iron pool [33, 75]. IONPs experience either a cytoplasmic or phagolysosome fate which can depend on the particle's size, surface charge, surface coating, and exposed cell/tissue type. Internalization of IONP particles within endosomes, lysosomes, or held in abiotic acidic conditions results in further oxidation and release of Fe^{2+} [75–77]. This potentially facilitated an increase in ROS in exposed SAECs by either interacting with the mitochondria membrane or catalyzing hydroxyl radical production via

hydrogen peroxide in acidic compartments [67, 68, 78]. In summary, it appears that IONPs' intracellular fate determines its solubility and ROS generation ability.

Acute exposure studies with SAEC-hTERTs found that nFe_2O_3 exposure altered SAEC iron homeostasis evidenced by increased expression of two major import proteins (CD71 and DMT1), increased intracellular Fe^{2+}, and ROS generation. In contrast, $nCeO_2$ exposure experienced CD71 over-expression, no change in intracellular iron, and a modest ROS increase. Interestingly, a separate *in vitro* $nCeO_2$ exposure (1 μg/cm^2) caused differential expression of CD71 to BEAS-2B cells at 24 h post-exposure [79], possibly indicating that $nCeO_2$ exposure may alter intracellular iron levels. For boundary layer epithelial cells between the external and internal environments, CD71 and DMT1 play important roles in iron uptake either through receptor-mediated endocytosis (i.e. CD71) or direct active transport across the membrane (DMT1). Iron in either phagolysosomes or CD71-containing endosomes solubilizes in the acidic environment, allowing for DMT1 to pump Fe^{2+} into the cytoplasm. In airway epithelium, FTH1 is found in the apical membrane to allow excess iron clearance via the mucociliary transport [34] and serves as the major intracellular storage protein to support the cytosolic labile iron pool with Fe^{2+} heavy chain and Fe^{3+} light chain storage. Although less is known about elimination, SLC40A1 plays an important role in pumping oxidized Fe^{3+} to the extracellular environment [74]. Normal epithelial cells exhibit relatively low CD71 and high ferriportin resulting in a small labile Fe pool [34]. Acute nFe_2O_3 exposure caused an increased ability to metabolize insoluble nFe_2O_3 resulting in a larger labile iron pool, with little evidence for altered elimination ability.

nFe_2O_3-transformed cells and clones displayed persistent over-expressed DMT1, decreased CD71 and FTH1, and increased intracellular iron compared to unexposed pSAECs suggesting that disruption of iron homeostasis over prolonged exposure shifted cells towards a larger labile iron pool and subsequent ROS generation. Similar findings, along with reduced SLC40A1 expression, in MWCNT clones suggests that persistent disruption of iron homeostasis may contribute to ENM-associated neoplastic-like transformation. Growing evidence supports the hypothesis that iron homeostasis disruption contributes to several cancer hallmarks, including genome stability, proliferation, energetics, and establishing the tumor microenvironment [37, 80]. Moreover, elevated iron levels and FTH1 expression [34] is a common observation following ultrafine iron or excessive particle inhalation exposure, iron overload in the lungs, and in cancer tissues. Elevated DMT1 or reduced CD71 expression can assist lung cancer cell lines to partly rely on high levels of soluble iron that fuels ROS generation, iron-dependent proteins, and processes that help fuel accelerated tumor proliferation and metastasis [34,37]. Iron overload in the lung or liver typically results in DMT1 over-expression. Since DMT1 is responsible for uptake of non-transferrin bound iron, it is likely that aberrant over-expression contributed to elevated iron in nFe_2O_3-tranformed cells. Moreover, it possibly contributed to soft agar colony formation ability in both nFe_2O_3 and MWCNT clones. Several proteins that are sensitive to ROS, iron levels, and are known tumor suppressor or enhancers possibly contributed to the observed changes in proteins involved in pSAEC iron transport. For example, p53 induction leads to increased FTH1 subunit and decreased CD71 expression [37, 74]. Our previous study identified over-expressed MYC as key proto-oncogene in MWCNT neoplastic-like transformation in SAECs [10]. Enhanced MYC expression can block FTH1 expression by over-expressing

IRP2, a key transcriptional regulator of iron homeostasis and may contribute to DMT1 over-expression [81]. Likewise, acute insoluble fiber exposure (e.g. asbestos) to human bronchoalveolar cells also showed elevated DMT1 and promotion of iron sequestration [34]. Next, many cancers exhibit a large labile iron pool due to suppressed FTH1 expression which appears to contribute to altered cell behavior, enhanced ROS, and tumorigenesis promotion [37]. *In vitro* exposure to dextran-coated γ-Fe_2O_3 nanoparticles caused increased levels of FTH1-stored iron and moderate ROS [82] while sub-chronic ferric ammonium citrate exposure, caused decreased in rat liver cell proliferation, soluble iron overload, and neoplastic transformation [83]. At present, our laboratory is currently conducting mechanistic time-response studies evaluating whether prolonged increases in labile iron contributes to increased and prolonged ROS switching cells from a oxidative damaged phenotype to a neoplastic-like phenotype.

With observed increased ROS, altered iron homeostasis in favor of excess intracellular Fe^{2+} iron, and cell immortalization, a growing literature base supports the hypothesis that long-term IONP exposure results in clastogenic initiating events and elevated tumorigenesis risk [33, 64]. A recent CometChip screening platform conducted on a series of VENGES-generated NMOs identified several metal oxide nanoparticles, including nFe_2O_3, harboring genotoxic potential [39]. Many *in vitro* exposure studies with different IONPs reported positive Comet assay, DNA damage products, and micronucleus frequency which associated with ROS induction [33, 38, 84, 85]. Conversely, other studies comparing Fe_2O_3 size-dependent effects report little genotoxicity or cell transformation in several mammalian cell lines [77, 86]. A systematic genotoxicity screening of several IONP particles in human lung cells has been initiated in our laboratory.

Responsible nanotechnology development will require adequate tiered toxicity screening workflows for numerous EMNs using *in vitro* and *in vivo* models for human risk assessment to support 'prevention by design' ENMs [15]. Since a majority of ENM exposures of concern are likely chronic in nature, chronic exposure screening models are still in their infancy [56] and current *in vitro* murine and immortalized human cell transformation models possess caveats and assumptions with their use. An ideal human *in vitro* cell model would exhibit a wild type epithelial phenotype, chromosomal stability, minimal damage to tumor enhancer/suppressor genes, and the ability to culture cells for an extended period of time. Use of this ideal model in a neoplastic transformation testing strategy could help identify both genotoxic and non-genotoxic tumorigenic ENMs, an already accepted, relatively reliable, and fast carcinogen screening paradigm [87].

Here, the pSAEC model allowed us to a) screen particles against a known ENM tumor promotor and b) isolate and re-culture soft agar clones from nFe_2O_3 and MWCNT exposed pSAECs that retained a majority of the neoplastic-like phenotype. Isolation and characterization of attached or unattached clones displaying enhanced tumor-like properties allows for further mechanistic study of tumorigenesis phenomena. Recent studies with isolated colonies or spheroids have proven valuable by identifying bi or multinucleated cells (i.e. mitotic disruption and genetic instability), tumorspheres, holoclones with stem cell characteristics, cancer stem-like cells, and CNT-induced malignant transformed cells [88,89]. The only caveat with the pSAEC model is that unexposed or untransformed

passaged cells exhibit a finite survival time, thus making mechanistic studies requiring large cells numbers difficult. With further refinement by adding genotoxicity screening, our pilot study using human pSAECs as an *in vitro* complete carcinogen - cell transformation assessment model may provide a novel tool for high throughput screening of ENMs for tumorigenesis risk.

5. Conclusions

We propose that pSAEC cells may serve as an additional ENM Tier I tumorigenesis screening model for alternative screening methods for an ENM tiered risk assessment framework. This model identified a VENGES-generated nFe_2O_3 as possessing neoplastic-like transformation ability, potentially through iron homeostasis disruption and elevated ROS levels, which were comparable to a MWCNT exposure, an established lung tumor promoter. The exposure model and use of sub-cultured clones can allow for screening and prioritization of numerous ENMs in shorter time spans (1 – 3 months) than traditional immortalized human cell transformation studies (4 – 6 months) and are not susceptible to issues with interspecies model comparisons. Further refinement of the proposed model to incorporate other cell types (e.g. macrophages) and acellular structure to simulate the tissue microenvironment will further enhance the predictability and accuracy of this sub-chronic *in vitro* model for ENM alternative testing strategies.

Supplementary Material

Refer to Web version on PubMed Central for supplementary material.

Acknowledgments

Abbreviations

DG	distorted grid
ENM	engineered nanomaterial
FESEM	field emission scanning electron microscope
hTERT	human telomerase reverse transcriptase
IONP	iron oxide nanoparticle
MWCNT	multi-walled carbon nanotube

nCeO₂	nano-scaled cerium oxide
nFe₂O₃	nano-scaled ferric oxide
NIOSH	National Institute for Occupational Safety and Health
NMO	nanometal oxide
OSHA PEL	Occupational Safety and Health Administration Permissible Exposure Limit
pSAEC	primary small airway epithelial cell
RID	Relevant *In vitro* Dosimetry
ROS	reactive oxygen species
SAGM	small airway cell growth medium
TEM	transmission electron microscope
VCM	Volumetric Centrifugation Method
VENGES	Versatile Engineered Nanomaterial Generating System

References

1. Nowack B, Brouwer C, Geertsma RE, Heugens EH, Ross BL, et al. Analysis of the occupational, consumer and environmental exposure to engineered nanomaterials used in 10 technology sectors. Nanotoxicology. 2013; 7:1152–1156. [PubMed: 22783888]

2. Pyrgiotakis, G., Vedantam, P., Cirenza, C., McDevitt, J., Eleftheriadou, M., Leonard, S., Demokritou, P. Optimization of a nanotechnology based antimicrobial platform for food safety applications using Engineered Water Nanostructures (EWNS); Scientific Reports. 2016. p. 1-12.http://doi.org/10.1038/srep21073

3. Roco, MC., Mirkin, CA., Hersam, MC. World Technology Evaluation Center Panel Report. National Science Foundation; 2010. Nanotechonology research directions for societal needs in 2020: retrospective and outlook; p. 607

4. Oberdorster G. Safety assessment for nanotechnology and nanomedicine: concepts of nanotoxicology. J Inter Med. 2010; 267(1):89–105.

5. Mercer RR, Scabilloni JF, Hubbs AF, Wang L, Battelli LA, et al. Extrapulmonary transport of MWCNT following inhalation exposure. Part Fibre Toxicol. 2013; 10:38. [PubMed: 23927530]

6. Zhu MT, Feng WY, Wang Y, Wang B, Wang M, Ouyang H, et al. Particokinetics and extrapulmonary translocation of intratracheally instilled ferric oxide nanoparticles in rats and the potential health risk assessment. Toxicol Sci. 2009; 107:342–351. [PubMed: 19023088]

7. Lu X, Miousse I, Pirela S, Moore J, Melnyk S, Koturbash I, Demokritou P. In vivo epigenetic effects induced by engineered nanomaterials: A case study of copper oxide and laser printer-emitted engineered nanoparticles. Nanotoxicology. 2015; 11:1–11.

8. Kuhlbusch TAJ, Asbach C, Fissan H, Gohler D, Stintz M. Nanoparticle exposure at nanotechnology workplaces: a review. Part Fibre Toxicol. 2011; 8:22. [PubMed: 21794132]

9. Hanahan D, Weinberg RA. Hallmarks of cancer: the next generation. Cell. 2011; 144:646–674. [PubMed: 21376230]

10. Wang L, Stueckle TA, Mishra A, Meighan T, Castranova V, Rojanasakul Y. Neoplastic-like transformation effect of single-walled and multi-walled carbon nanotubes vs. asbestos in human small airway epithelial cells. Nanotoxicology. 2014; 8:485–507. [PubMed: 23634900]

11. Siegrist KJ, Reynolds SH, Kashon ML, Lowry DT, Dong C, Hubbs AF, et al. Genotoxicity of multi-walled carbon nanotubes at occupationally relevant doses. Part Fibre Toxicol. 2014; 11:6. [PubMed: 24479647]

12. Khatri M, Bello D, Pal AK, Cohen JM, Woskie S, Gassert T, et al. Evaluation of cytotoxic, genotoxic and inflammatory responses of nanoparticles from photocopiers in three human cell lines. Part Fibre Toxicol. 2013; 10:42. [PubMed: 23968360]

13. Snyder-Talkington BN, Dymacek J, Porter DW, Wolfarth MG, Mercer RR, Pacurari M, Denvir H, Castranova V, Qian Y, Guo NL. System-based identification of toxicity pathways associated with multi-walled carbon nanotube-induced pathological responses. Toxicol Appl Pharmacol. 2013; 272:476–489. [PubMed: 23845593]

14. Kumar A, Dhawan A. Genotoxic and carcinogenic potential of engineered nanoparticles: an update. Arch Toxicol. 2013; 87:1883–1900. [PubMed: 24068037]

15. Nel AE, Nasser E, Godwin H, Avery D, Bahadori T, et al. A multi-stakeholder perspective on the use of alternative test strategies for nanomaterial safety assessment. ACS Nano. 2013; 7(8):6422–33. [PubMed: 23924032]

16. Curwin B, Bertke S. Exposure characterization of metal oxide nanoparticles in the workplace. J Occupat Environ Hyg. 2011; 8:580–587.

17. Brenner SA, Neu-Baker NM, Caglayan C, Zurbenko IG. Occupational exposure to airborne nanomaterials: an assessment of worker exposure to aerosolized metal oxide nanoparticles in semiconductor wasterwater treatment. J Occupat Environ Hyg. 2015; 12:469–481.

18. Methner M, Hodson L, Dames A, Geraci C. Nanoparticle emission assessment technique (NEAT) for the identification and measurement of potential inhalation exposure to engineered nanomaterials-Part B: results from 12 field studies. J Occup Environ Hyg. 2010; 7:163–176. [PubMed: 20063229]

19. Pirela S, Lu X, Miousse I, Sisler J, Qian Y, Guo L, Koturbash I, Castranova V, Thomas T, Godleski J, Demokritou P. Effects of intratracheally instilled laser printer-emitted engineered nanoparticles in a mouse model: A case study of toxicological implications from nanomaterials released during consumer use. NanoImpact. 2016; 1:1–8. [PubMed: 26989787]

20. Teeguarden JG, Mikheev VB, Minard KR, Forsythe WC, Wang W, Sharma G, Karin N, Tilton SC, Waters KM, Asgharian B, Price OR, Pounds JG, Thrall BD. Comparative iron oxide nanoparticle cellular dosimetry and response in mice by the inhalation and liquid cell culture exposure routes. Part Fibre Toxicol. 2014; 11:46. [PubMed: 25266609]

21. Ma JY, Mercer RR, Barger M, Schwegler-Berry D, Scabilloni J, Ma JK, Castranova V. Induction of pulmonary fibrosis by cerium oxide nanoparticles. Toxicol Appl Pharmacol. 2012; 262(3):255–264. [PubMed: 22613087]

22. Cassee FR, van Balen EC, Singh C, Green D, Muijser H, Weinstein J, Dreher K. Exposure, health and ecological effects review of engineered nanoscale cerium and cerium oxide associated with its use as a fuel additive. Crit Rev Toxicol. 2011; 41(3):213–229. [PubMed: 21244219]

23. Health Effects Institute (HEI). Evaluation of human health risk from cerium added to diesel fuel. In: Hibbs, JB., Jr, editor. HEI Communication. Vol. 9. Boston MA, USA: Integrated Laboratory Systems; 2001. Infection and nitric oxide. J Infect Dis. 2002; 185(suppl 1):S9:17. [PubMed: 11865435]

24. Ma JY, Zhao H, Mercer RR, Barger M, Rao M, Meighan T, Schwegler-Berry D, Castranova V, Ma JK. Cerium oxide nanoparticle-induced pulmonary inflammation and alveolar macrophage functional changes in rats. Nanotoxicology. 2011; 5:312–325. [PubMed: 20925443]

25. Demokritou P, Gass S, Pyrgiotakis G, Cohen JM, Goldsmith W, McKinney W, Frazer D, Ma J, Schwegler-Berry D, Brain J, Castranova V. An in vivo and in vitro toxicological characterisation of realistic nanoscale CeO2 inhalation exposures. Nanotoxicology. 2013; 7:1338–1350. [PubMed: 23061914]

26. Gosens I, Mathijssen LE, Bokkers BG, Muijser H, Cassee FR. Comparative hazard identification of nano- and micro-sized cerium oxide particles based on 28-day inhalation studies in rats. Nanotoxicology. 2014; 8(6):643–653. [PubMed: 23768316]

27. Yokel R, Hussain S, Garantziotis S, Demokritou P, Castranova V, Cassee F. The Yin: an adverse health perspective of nanoceria: uptake, distribution, accumulation, and mechanisms of its toxicity. Environ Science Nano. 2014; 1:406–425.

28. Peng L, He X, Zhang P, Zhang J, Li Y, et al. Comparative pulmonary toxicity of two ceria nanoparticles with the same primary size. Int J Mol Sci. 2014; 15:6072–6085. [PubMed: 24727375]

29. Benameur L, Auffan M, Cassien M, Liu W, Culcasi M, Rahmouni H, Stocker P, Tassistro V, Bottero JY, Rose J, Botta A, Pietri S. DNA damage and oxidative stress induced by CeO2 nanoparticles in human dermal fibroblasts: Evidence of a clastogenic effect as a mechanism of genotoxicity. Nanotoxicology. 2015; 9(6):696–705. [PubMed: 25325158]

30. Hashem RM, Rashd LA, Hashem KS, Soliman HM. Cerium oxide nanoparticles alleviate oxidative stress and decreases Nrf-2/HO-1 in D-GALN/LPS induced hepatotoxicity. Biomed Pharmacother. 2015; 73:80–86. [PubMed: 26211586]

31. Lundgren DL, Hahn FF, Griffith WC, Hubbs AF, Nikula KJ, et al. Pulmonary carcinogenicity of relatively low doses of beta-particle radiation from inhaled 144CeO2 in rats. Radiat Res. 1996; 146(5):525–535. [PubMed: 8896579]

32. Soenen SJ, De Cuyper M, De Smedt SC, Braeckmans K. Investigating the toxic effects of iron oxide nanoparticles. Meth Enzym. 2012; 509:195–224. [PubMed: 22568907]

33. Valdiglesias V, Kilic G, Costa C, Fernandez-Bertolez N, Pasaro E, Teixeira JP, Laffon B. Effects of iron oxide nanoparticles: cytotoxicity, genotoxicity, developmental toxicity, and neurotoxicity. Environ Mole Mutag. 2015; 56:125–148.

34. Ghio AJ. Disruption of iron homeostasis and lung disease. Biochem et Biophysica Acta. 2009; 1790:731–739.

35. Andujar P, Simon-Deckers A, Galateau-Salle F, et al. Role of metal oxide nanoparticles in histopathological changes observed in the lung of welders. Part Fibre Toxicol. 2014; 11:23. [PubMed: 24885771]

36. Toyokuni S. Role of iron in carcinogenesis: cancer as a ferrotoxic disease. Cancer Sci. 2009; 100:9–16. [PubMed: 19018762]

37. Torti SV, Torti FM. Iron and cancer: more ore to be mined. Nat Rev Cancer. 2013; 13:342–55. [PubMed: 23594855]

38. Ishino K, Kato T, Kato M, Shibata T, Watanabe M, et al. Comprehensive DNA adduct analysis reveals pulmonary inflammatory response contributes to genotoxic action of magnetite nanoparticles. Int J Mol Sci. 2015; 16:3472–3492.

39. Watson C, Ge J, Cohen J, Pyrgiotakis G, Engelward BR, Demokritou P. High-throughput screening platform for engineered nanoparticle-mediated genotoxicity using comet chip technology. ACS Nano. 2014; 8:2118–2133. [PubMed: 24617523]

40. Suzui M, Futakuchi M, Fukamachi K, Numano T, Abdelgied M, et al. Multiwalled carbon nanotubes intratracheally instilled into the rat lung induce development of pleural malignant mesothelioma and lung tumors. Canc Sci. 2016; 107:924–935.

41. Sargent LM, Porter DW, Staska LM, Hubbs A, Lowry D, et al. Promotion of lung adenocarcinoma following inhalation exposure to multi-walled carbon nanotubes. Part Fibre Toxicol. 2014; 11:3. [PubMed: 24405760]

42. Creton S, Aardema MJ, Carmichael PL, Harvey JS, Martin FL, et al. Cell transformation assays for prediction of carcinogenic potential: state of the science and future research needs. Mutag. 2012; 1:93–101.

43. Demokritou P, Buchel R, Molina RM, Deloid GM, Brain JD, Pratsinis SE. Development and characterization of a versatile engineered nanomaterial generation system (VENGES) suitable for toxicological studies. Inhal Toxciol. 2010; 22:107–116.

44. Sotiriou GA, Diaz E, Long MS, Godleski J, Brain J, Pratsinis SE, Demokritou P. A novel platform for pulmonary and cardiovascular toxicological characterization of inhaled engineered nanoparticles. Nanotoxicology. 2012; 6:680–690. [PubMed: 21809902]

45. Gass S, Cohen JM, Pyrgiotakis G, Sotiriou GA, Pratsinis SE, Demokritou P. A safer formulation concept for flame-generated engineered nanomaterials. ACS Sustain Chem Eng. 2013; 1:843–857. [PubMed: 23961338]

46. Porter DW, Hubbs AF, Mercer RR, Wu N, Wolfarth MG, Sriram K, et al. Mouse pulmonary dose- and time course-responses induced by exposure to multi-walled carbon nanotubes. Toxicology. 2010; 269:136–147. [PubMed: 19857541]

47. Cohen J, Deloid G, Pyrgiotakis G, Demokritou P. Interactions of engineered nanomaterials in physiological media and implications for in vitro dosimetry. Nanotoxicology. 2013; 7:417–31. [PubMed: 22393878]

48. Cohen J, Deloid G, Pyrgiotakis G, Demokritou P. Interactions of engineered nanomaterials in physiological media and implications for in vitro dosimetry. Nanotoxicology. 2013; 7:417–31. [PubMed: 22393878]

49. DeLoid G, Cohen JM, Darrah T, Derk R, Rojanasakul L, Pyrgiotakis G, Wohlleben W, Demokritou P. Estimating the effective density of engineered nanomaterials for in vitro dosimetry. Nat Commun. 2014; 5:3514. [PubMed: 24675174]

50. Cohen J, Teeguarden J, Demokritou P. An integrated approach for the in vitro dosimetry of engineered nanomaterials. Part Fibre Toxicol. 2014; 11:20. [PubMed: 24885440]

51. DeLoid GM, Cohen JM, Pyrgiotakis G, Pirela SV, Pal A, Liu J, Srebric J, Demokritou P. Advanced computational modeling for in vitro nanomaterial dosimetry. Part Fibre Toxicol. 2015; 12:32. [PubMed: 26497802]

52. Pongrakhananon V, Luanpitpong S, Stueckle TA, Wang L, Nimmannit U, Rojanasakul Y. Carbon nanotubes induce apoptosis resistance of human lung epithelial cells through FLICE-inhibitory protein. Toxicol Sci. 2015; 143:499–511. [PubMed: 25412619]

53. Lamouille S, Xu J, Derynck R. Molecular mechanisms of epithelial-mesenchymal transition. Nat Rev Mole Cell Biol. 2014; 15:178–196.

54. Ponti J, Colognato R, Rauscher H, Gioria S, Broggi F, et al. Colony forming efficiency and microscopy analysis of multi-walled carbon nanotubes cell interaction. Toxicol Lett. 2010; 197:29–37. [PubMed: 20435104]

55. Sasaki K, Bohnenberger S, Hayashi K, Kunkelmann T, Muramatsu D, et al. Photo catalogue for the classification of foci in the BALB/c 3T3 cell transformation assay. Mut Res. 2012; 744:42–53. [PubMed: 22331008]

56. Becker H, Herzberg F, Schulte A, Kolossa-Gehring M. The carcinogenic potential of nanomaterials, their release from products and options for regulating them. Int J Hyg Environ Health. 2011; 214:231–238. [PubMed: 21168363]

57. Nymark P, Jensen KA, Suhonen S, Kembouche Y, Vippola M, et al. Free radical scavenging and formation by multi-walled carbon nanotubes in cell free conditions and in human bronchial epithelial cells. Part Fibre Toxicol. 2014; 11:4. [PubMed: 24438343]

58. Naganuma T, Traversa E. The effect of cerium valence states at cerium oxide nanoparticle surfaces on cell proliferation. Biomaterials. 2014; 35:4441–53. [PubMed: 24612920]

59. Wason MS, Zhao J. Cerium oxide nanoparticles: potential applications for cancer and other diseases. Am J Transl Res. 2013; 5:126–131. [PubMed: 23573358]

60. Pagliari F, Mandoli C, Forte G, Magnani E, Pagliari S, et al. Cerium oxide nanoparticles protect cardiac progenitor cells from oxidative stress. ACS Nano. 2012; 6:3767–75. [PubMed: 22524692]

61. Heckert E, Seal S, Self WT. Fenton-like reaction catalyzed by the rare earth inner transition metal cerium. Environ Sci Tehcnol. 2008; 42:5014–19.

62. Sighinolfi GL, Artoni E, Gatti AM, Corsi L. Carcinogenic potential of metal nanoparticles in BALB/3T3 cell transformation assay. Environ Toxicol. 2016; 31:509–19. [PubMed: 25358123]

63. Combes R, Balls M, Curren R, Fischbach M, Fusenig N, et al. Cell transformation assays as predictors of human carcinogenicity. ATLA. 1999; 27:745–767. [PubMed: 25490287]

64. Dissanayake NM, Current KM, Obare SO. Mutagenic effects of iron oxide nanoparticles on biological cells. Int J Mol Sci. 2015; 16:23482–516. [PubMed: 26437397]

65. Elias Z, Poirot O, Schneider O, Marande AM, Daniere MC, Terzetti F, Perzerat H, Fournier J, Zalma R. Cytotoxic and transforming effects of some iron-containing minerals in Syrian hamster embryo cells. Cancer Detect Prev. 1995; 19:405–414. [PubMed: 7585726]

66. Saffiotti U, Ahmed N. Neoplastic transformation by quartz in the BALB/3T3/A31-1-1 cell line and the effects of associated minerals. Teratog Carcinog Mutagen. 1995; 15:339–56. [PubMed: 8732883]

67. Chen Z, Yin JJ, Zhou YT, Zhang Y, Song L, et al. Dual enzyme-like activities of iron oxide nanoparticles and their implication for diminishing cytotoxicity. ACS Nano. 2012; 6:4001–12. [PubMed: 22533614]

68. Shukla S, Jadaun A, Arora V, Sinha RK, Biyani N, Jain VK. In vitro toxicity assessment of chitosan oligosaccharide coated iron oxide nanoparticles. Toxicol Reports. 2015; 2:27–39.

69. Zhang T, Qi Y, Liao M, Xu M, Bower KA, Frank JA, Shen HM, Luo J, Shi X, Chen G. Autophagy is a cell self-protective mechanism against arsenic-induced cell transformation. Toxicol Sci. 2012; 130:298–308. [PubMed: 22869613]

70. Steenland K, Beaumont J, Elliot L. Lung cancer in mild steel welders. Am J Epidemiol. 1991; 133:220–229. [PubMed: 2000839]

71. Moulin JJ, Wild P, Haguenoer JM, Faucon D, DeGaudemaris R, et al. A mortality study amoung mild steel and stainless steel workers. Br J Ind Med. 1993; 50:234–243. [PubMed: 8457490]

72. Zhu MT, Feng WY, Wang B, Wang TC, Gu YQ, et al. Comparative study of pulmonary responses to nano- and submicron-sized ferric oxide in rats. Toxicology. 2008; 247:102–111. [PubMed: 18394769]

73. Sadeghi L, Babadi VY, Espanani HR. Toxic effects of the Fe2O3 nanoparticles on the liver and lung tissue. Bratisl Lek Listy. 2015; 116:373–378. [PubMed: 26084739]

74. Zhang C, Zhang F. Iron homeostasis and tumorigenesis: molecular mechanisms and therapeutic opportunities. Protein Cell. 2015; 6:88–100. [PubMed: 25476483]

75. Soenen SJH, De Cuyper M. Assessing iron oxide nanoparticle toxicity in vitro: current status and future prospects. Nanomed. 2010; 5:1261–1275.

76. Zhu MT, Wang Y, Feng WY, Wang B, Wang M, Ouyang H, Chai ZF. Oxidative stress and apoptosis induced by iron oxide nanoparticles in cultured human umbilical endothelial cells. J Nanosci Nanotechnol. 2010; 10:8584–90. [PubMed: 21121369]

77. Freyria FS, Bonelli B, Tomatis M, Ghiazza M, Gazzano E, et al. Hematite nanoparticles larger than 90 nm show no sign of toxicity in terms of lactate dehydrogenase release, nitric oxide generation, apoptosis, and comet assay in murine alveolar macrophages and human lung epithelial cells. Chem Res Toxicol. 2012; 25:850–861. [PubMed: 22324577]

78. Sohn YS, Ghoti H, Breuer W, Rachmilewitz E, Attar S, Weiss G, Cabantchik ZI. The role of endocytic pathways in cellular uptake of plasma non-transferrin iron. Haematologica. 2012; 94:670–8.

79. Verstraelen S, Remy S, Casals E, De Boever P, Witters H, et al. Gene expression profiles reveal distinct immunological responses of cobalt and cerium dioxide nanoparticles in two in vitro lung epithelial cell models. Toxicol Lett. 2014; 228:157–169. [PubMed: 24821434]

80. Jung M, Mertens C, Brune B. Macrophage iron homeostasis and polarization in the context of cancer. Immunobiology. 2015; 220:295–304. [PubMed: 25260218]

81. Wu KJ, Polack A, Dalla-Favera R. Coordinated regulation of iron-controlling genes, H-ferritin and IRP2, by c-Myc. Science. 1999; 283:676–679. [PubMed: 9924025]

82. Geppert M, Hohnholt MC, Nurnberger S, Dringen R. Ferritin up-regulation and transient ROS production in cultured brain astrocytes after loading with iron oxide nanoparticles. Acta Biomater. 2012; 8:3832–3839. [PubMed: 22750736]

83. Messner DJ, Kowdley KV. Neoplastic transformation of rat liver epithelial cells is enhanced by non-transferrin-bound iron. BMC Gastroenterol. 2008; 8:2. [PubMed: 18254965]

84. Bhattacharya K, Davoren M, Boertz J, Schins RP, Hoffmann E, Dopp E. Titanium dioxide nanoparticles induce oxidative stress and DNA-adduct formation but not DNA-breakage in human lung cells. Part Fibre Toxicol. 2009; 6:17. [PubMed: 19545397]

85. Singh N, Jenkins GJS, Nelson BC, Marquis BJ, Maffeis TG, et al. The role of iron redox state in the genotoxicity of ultrafine superparamagnetic iron oxide nanoparticles. Biomaterials. 2012; 33:163–170. [PubMed: 22027595]

86. Guichard Y, Schmit J, Darne C, Gate L, Goutet M, et al. Cytotoxicity and genotoxicity of nanosized and microsized titanium dioxide and iron oxide particles in Syrian hamster embryo cells. Ann Occup Hyg. 2012; 56:631–644. [PubMed: 22449629]

87. Benigni R. Alternatives to the carcinogenicity bioassay for toxicity prediction: are we there yet? Expert Opin Drug Metab Toxicol. 2012; 8:4.

88. Luanpitpong S, Wang L, Castranova V, Rojanasakul Y. Induction of stem-like cells with malignant properties by chronic exposure of human lung epithelial cells to single-walled carbon nanotubes. Part Fibre Toxicol. 2014; 11:22. [PubMed: 24885671]

89. Weiswald LB, Bellet D, Dangles-Marie V. Spherical cancer models in tumor biology. Neoplasia. 2015; 17:1–15. [PubMed: 25622895]

6. Appendices

Appendix A – Supplemental Methods. Figures B.1 – B.9.

Highlights

- This study investigated and compared bio-effects of long-term (10 weeks) *in vitro* exposure of $nCeO_2$ and nFe_2O_3 *vs.* MWCNT in human primary small airway epithelial cells.

- Nanoparticle dosimetry and intracellular uptake were determined using distorted grid modeling, enhanced darkfield, and TEM microscopy.

- Sub-chronic exposure to nano-scaled metal oxides resulted in 30% deposition of the administered dose resulting in phagocytosis or cytoplasm fate.

- nFe_2O_3 and MWCNT caused increased proliferation, invasion, and colony formation indicating neoplastic-like transformation.

- Increased intracellular iron, ROS, and iron homeostasis disruption may be the mechanisms potentially contributing to cell transformation.
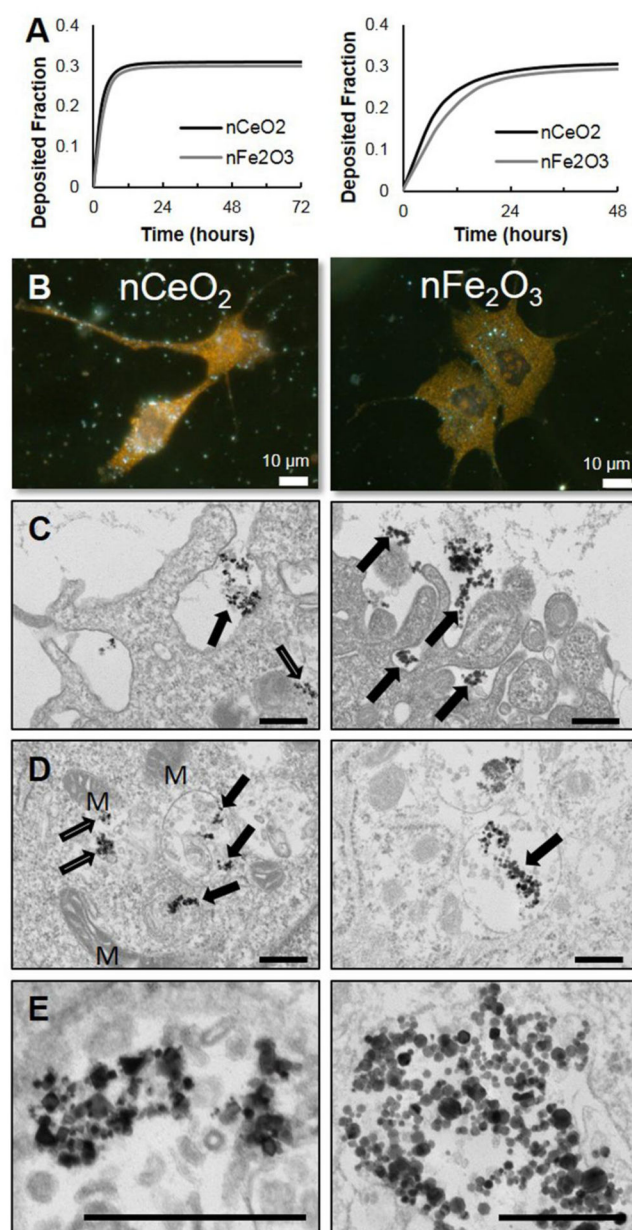
Figure 1.

Dosimetry modeling, cellular fate, and co-localization of $nCeO_2$ and nFe_2O_3 particles via enhanced darkfield and transmission electron microscopy following exposure in primary human small airway epithelial cells. A) Harvard distorted grid modeling of sub-chronic exposure in 6-well plates (left) and acute exposure in 96-well plates (right). B) Cells plated on medium-conditioned glass slides were exposed for 48 h in 24-well plates to $nCeO_2$ (left) and nFe2O3 (right; 0.017 μg/cm^2 deposited). Both nanometal oxides were found co-localized in cytoplasm. Bars = 10 μm. C) Following 24 h exposure to 0.18 μg/cm^2, both $nCeO_2$ and nFe_2O_3 were observed to undergo internalization via phagocytosis (black arrows) and the cell membrane periphery. D) $nCeO_2$ was observed both in the cytoplasm

(white arrows) and enclosed in membrane-bound vesicles (black arrows). nFe_2O_3 particles were exclusively found in membrane-bound vesicles. 'M' signifies mitochondria. E) Both NMO were found as loose agglomerates within exposed cells. Bars = 400 nm.
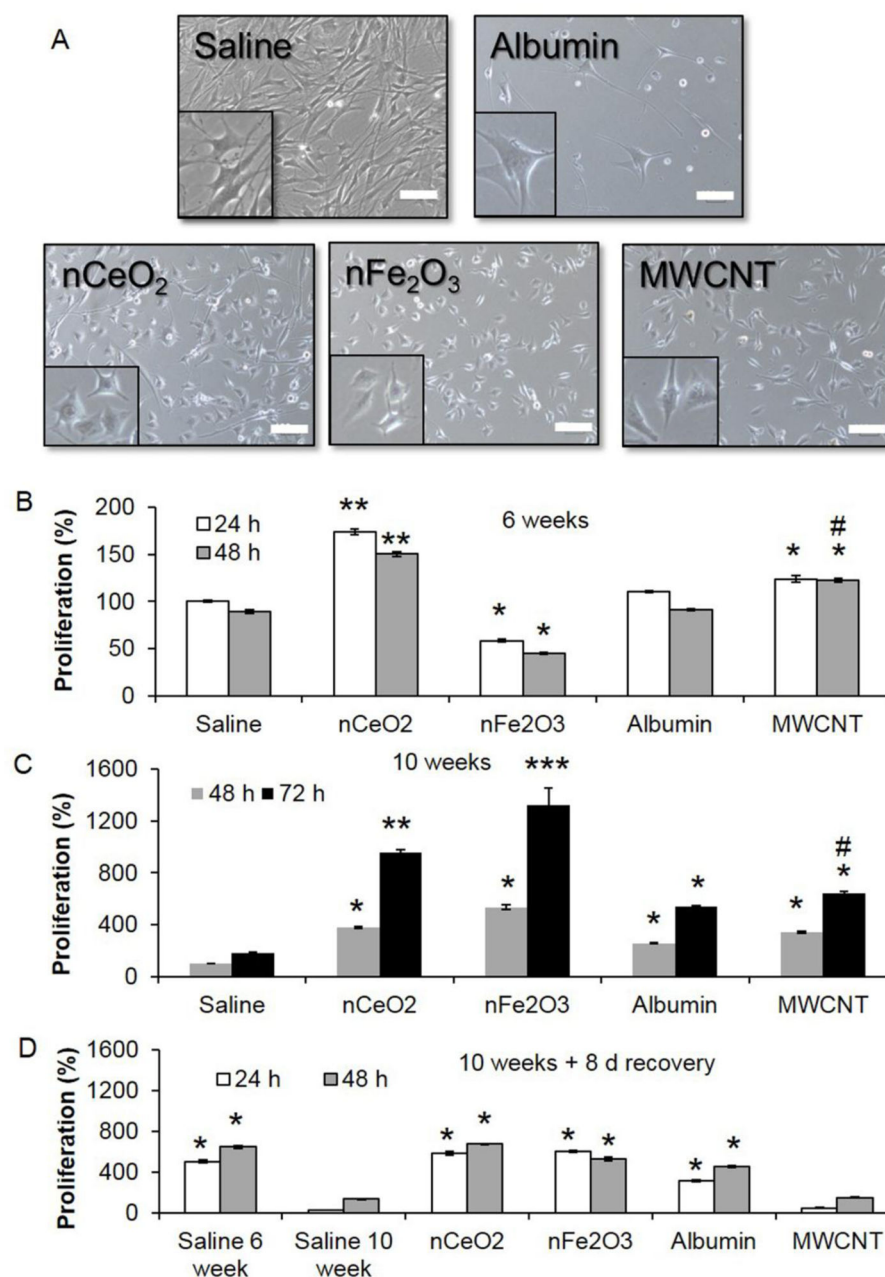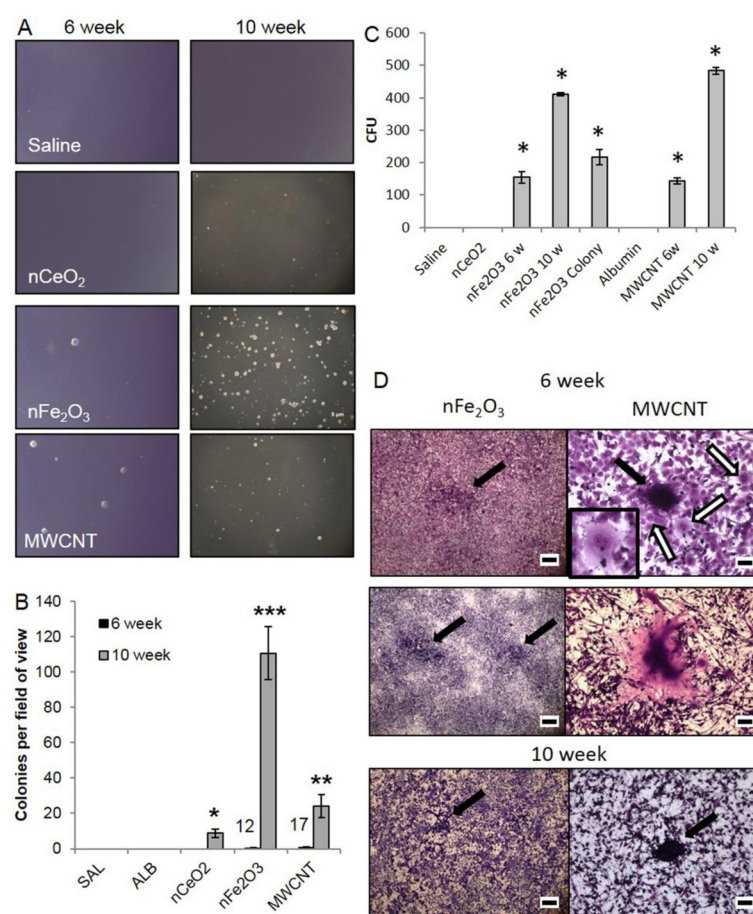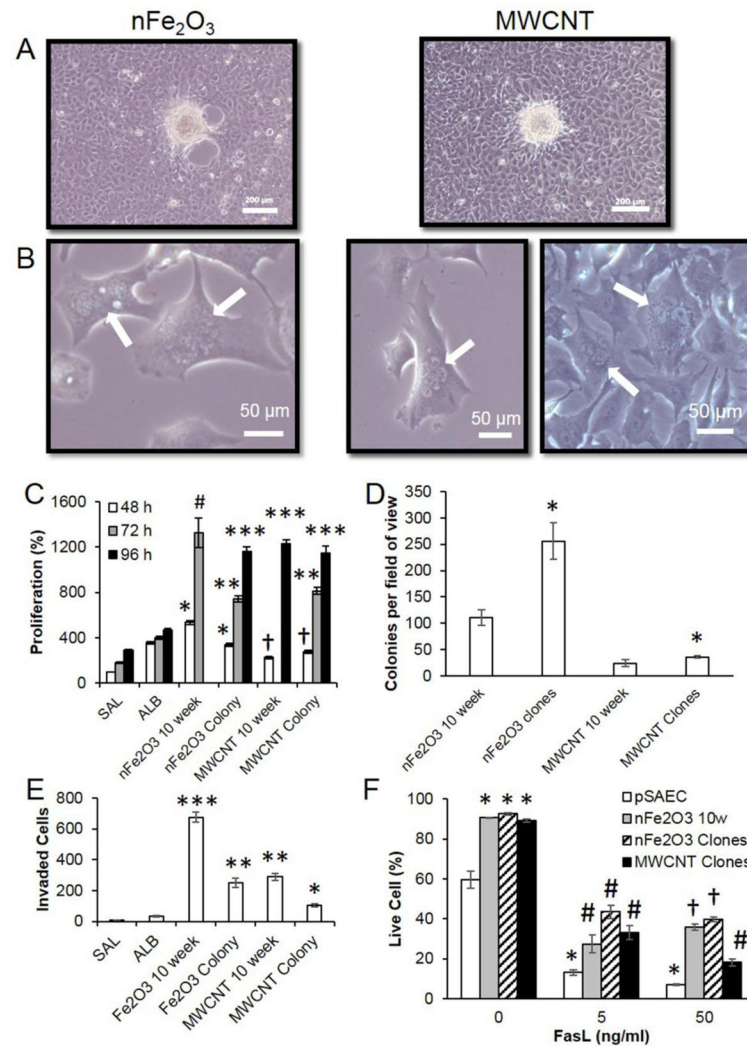
Figure 2.
Cell morphology and cell proliferation of $nCeO_2$, nFe_2O_3, and MWCNT-exposed pSAECs at 6 and 10 weeks after 0.18 μg NMO/cm^2 and 0.06 μg MWCNT/cm^2 exposures. A) At 48 h post-seeding, $nCeO_2$, nFe_2O_3, and MWCNT exposed cells displayed a more rounded morphology compared to saline passage and low passage pSAECs. Bars and insert width = 200 μm. B) At 6 weeks exposure, $nCeO_2$-and MWCNT-exposed cells increased cell proliferation, as measured by WST-1 assay, above respective controls while nFe_2O_3-exposed cells experienced a significant reduction. C) At 10 weeks exposure, nFe_2O_3-exposed cells possessed the largest significant increase in cell proliferation compared to all treatments. D) Following 8 days recovery in particle-free medium, both $nCeO_2$ and nFe_2O_3 retained

significantly elevated proliferation, while MWCNT-exposed cells exhibited a significant decrease compared to albumin-only (dispersant control) exposed cells. * and # indicate significant difference (p   0.05) compared to saline control and albumin-only exposed cells, respectively.

Figure 3.
Cell transformation evidenced by attachment independent and dependent colonies in nFe$_2$O$_3$- and MWCNT-exposed pSAECs. A) Representative micrographs of 6 and 10 week exposed cells to nCeO$_2$, nFe$_2$O$_3$, and MWCNT compared to saline- and albumin-exposed (not shown) cells. B) Mean counts of colonies displaying attachment-independent growth in soft agar assay. Primary SAECs were exposed for 6 and 10 weeks, passaged, and then plated onto solidified agar supplemented with culture growth factors and 15% FBS. At Day 21, triplicate plates per population were counted and pooled. Numbers above 6 week mean counts indicate the total number of colonies observed over three replicates. C) nFe$_2$O$_3$ and MWCNT colony forming unit counts for 6 and 10 week transformed and soft agar clones. * indicates significant difference compared to saline and albumin passage controls ($p < 0.05$). D) Type I foci (black arrows) in nFe$_2$O$_3$- and MWCNT-exposed pSAECs at 6 week exposure. Scale bar = 5 mm. Small Type II foci in nFe$_2$O$_3$-exposed cells at 6 weeks surrounded by several bi-nucleated cells (white arrows; inset). Scale bar = 100 μm. Abnormal 'giant cells' were observed in MWCNT-exposed pSAECs. Scale bar = 100 μm. Small Type II focus in 10 week exposed nFe$_2$O$_3$ pSAECs (scale bar = 5 mm) and MWCNT pSAECs (scale bar = 100 μm).

Figure 4.
Subclones from 10 week nFe_2O_3 and MWCNT-exposed pSAEC soft agar colonies retained transformation and several cancer cell hallmark characteristics. A) Plated subclones exhibited foci in confluent plates. B) Multi-nucleated cells were observed in both sub-clone populations. C) Retention of accelerated proliferation compared to 10 week exposure populations, saline-(SAL), and albumin (ALB)-exposed cells, respectively. nFe_2O_3 10 week absorbance values exceeded detection values at 96 h time point. nFe_2O_3- and MWCNT-exposed cells are compared to their respective vehicle control-exposed cells. Different * and # symbols indicate significant differences compared to other treatment groups at each time point. † indicates a significant decrease compared to ALB control (p ≤ 0.05). D) Both nFe_2O_3 and MWCNT clones exhibited significant increases (*, $p < 0.05$) in the number of soft agar colonies and E) significant decreases in invasion ability compared to their 10 week transformed counterparts, but above SAL-, and ALB-exposed cells' ability. F) Enhanced apoptosis resistance of nFe_2O_3- and MWCNT-exposed cells in the extrinsic pathway compared to low passage pSAECs. Cells were exposed to FasL for 24 h, fluorescently

labeled, and imaged on the ImageXpress. Symbols indicate statistical significance from unexposed pSAEC (*), pSAEC (#) and all other treatment (+) ($p < 0.05$, n=4).
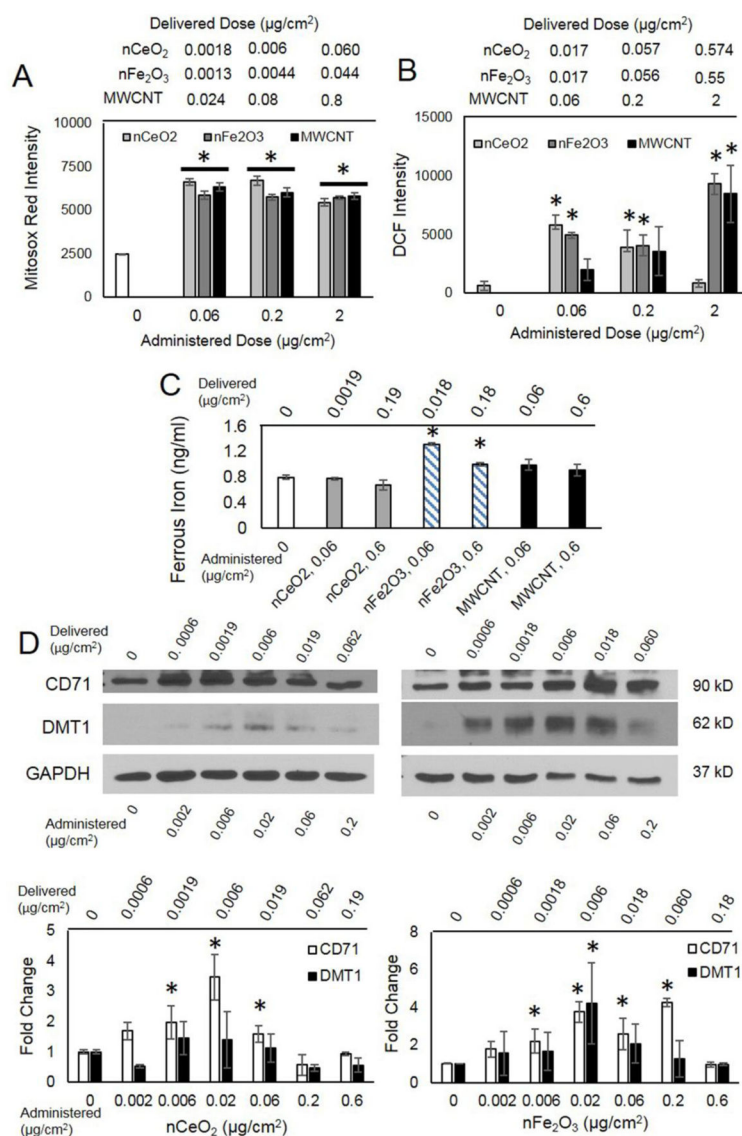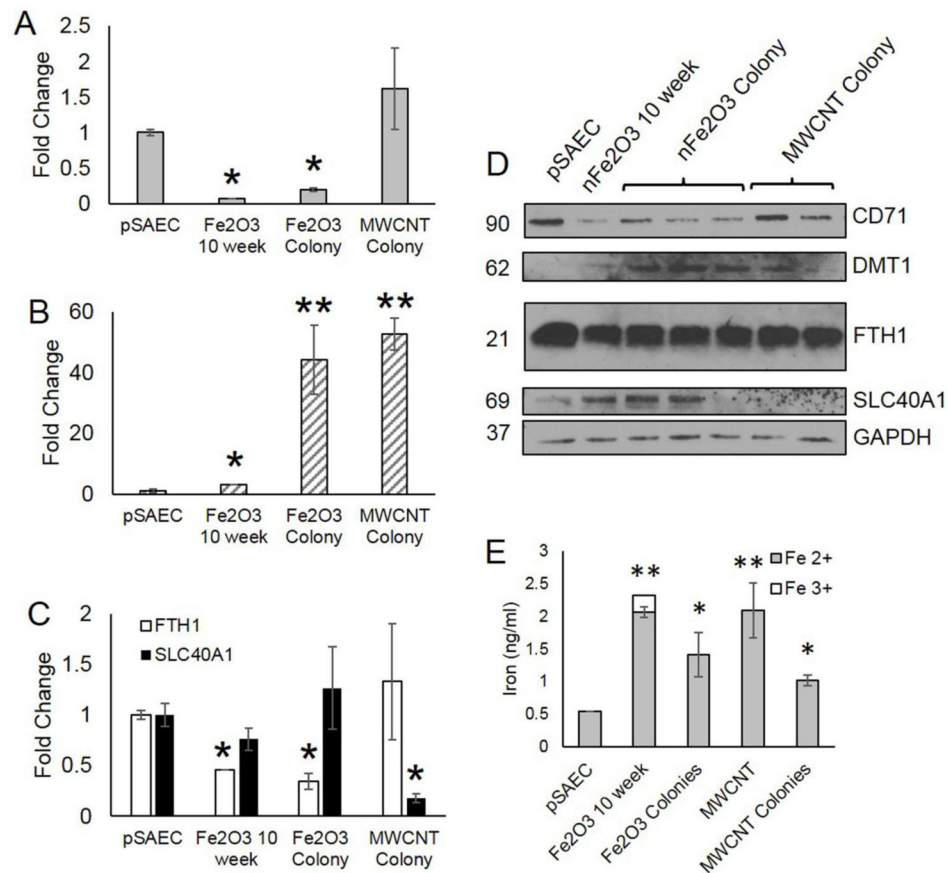
Figure 5.
ROS generation and iron homeostasis disruption in nFe$_2$O$_3$-exposed SAECs. A) Superoxide production at 1 h (Mitosox Red) and B) ROS levels (DCF) intensity quantification after 24 h exposure in pSAECs. C) Ferrous iron intracellular concentrations following acute 24 h exposure in SAEC-hTERT. D) Enhanced transferrin receptor (CD71) and divalent metal transporter 1 (DMT1) expression following 24 h acute exposure to nCeO$_2$ and nFe$_2$O$_3$ in SAEC-hTERTs. MWCNT dosimetry was based off of data reported by Wang et al. 2010 and Nymark et al. 2014. * indicate a significant difference compared to unexposed and other exposed treatment groups (p<0.05).

Figure 6.
Altered iron homeostasis protein expression and increased intracellular iron levels in nFe$_2$O$_3$-transformed cells and colony clones. A) Decreased transferrin receptor (CD71) and B) increased divalent metal transporter (DMT1) expression in nFe$_2$O$_3$-transformed cells and clones compared to low passage, unexposed pSAECs. C) Decreased ferritin (FTH1) expression in nFe$_2$O$_3$-transformed cells and clones. D) Representative protein bands via SDS-page Western Blot. All densitometry quantification used GAPDH as a loading control. E) Increased intracellular ferrous iron in ENM sub-chronic exposed pSAECs. * indicate a significant difference compared to low passage pSAEC control (p<0.05).

Table 1

Size, BET surface area, and suspension characterization for each ENM.

Material	Manufacturer	Process	d_{XRD} (nm)	d_{BET} (nm)	Length (μm)	SSA (m²/g)
nCeO₂	Harvard University	VENGES FSP	23.7	33.6	n/a	59
nFe₂O₃	Harvard University	VENGES FSP	12.2	11.9	n/a	96
MWCNT Mitsui #7	Hodagoya Chemical	CVD	8.2	n/a	8.1 ±5	26

dXRD = x-ray diffraction, dBET = diameter based on surface area/density, SSA = specific surface area.

Author Manuscript Author Manuscript Author Manuscript Author Manuscript

Table 2

Properties of particle dispersions in small airway epithelial cell growth medium (SAGM). d_H: hydrodynamic diameter, PdI: polydispersity index, ζ: zeta potential, σ: specific conductance, ρ_{agg}: agglomerate effective density.

Material	Media	Intensity-weighted d_H in water (nm)	Intensity-weighted d_H (nm)	Volume-weighted d_H (nm)	PdI	ζ water (mV)	ζ medium (mV)	σ (mS/cm)	ρ_{agg} (g/cm³)
$nCeO_2$	SAGM	734 ±97.6	241 ±9.53	341.19 ± 41.01	0.401 ± 0.013	−10.0 ±1.5	−10.8 ±2.5	8.76 ± 0.42	1.754 ± 0.075
nFe_2O_3	SAGM	74 ±0.6	214.9 ±1.8	341.56 ± 51.95	0.271 ± 0.009	25.3 ±1.7	−11.4 ±3.5	11.10 ± 0.08	1.691 ± 0.053
MWCNT Mitsui #7	SAGM	n/a	78	ND	ND	−40.6	−8.41	ND	ND

Values represent the mean (± SD) of a triplicate reading. All values are for SAGM medium, unless otherwise noted by column heading. ND = not determined.

Table 3

Delivered dose metrics and relevant *in vitro* (RID) doses for various ENMs dispersions in SAGM.

Material	Exposure conditions				α_1	α_2	RID_M (g)	RID_N (#)	RID_{SA} (cm^2)
	Well layout	Administered Dose (μg/ml)	Volume (ml)	Duration (hours)					
nCeO$_2$	6	0.096	2	72	0.3092	0.3605	0.058	1.598E+12	5844
	6	2.88	2	72	0.3092	0.3605	1.749	4.794E+13	175308
	96	0.096	0.2	48	0.3036	0.1266	0.006	1.594E+11	583
	96	0.96	0.2	48	0.3036	0.1266	0.058	1.594E+12	5831
nFe$_2$O$_3$	6	0.096	2	72	0.2995	0.2916	0.058	1.632E+12	5982
	6	2.88	2	72	0.2995	0.2916	1.728	4.896E+13	179460
	96	0.096	0.2	48	0.3002	0.09685	0.006	1.618E+11	593
	96	0.96	0.2	48	0.3002	0.09682	0.057	1.618E+12	5930

Values represent the mean (± SD) of a triplicate reading. The following equation, $f(x) = \alpha 1\ (1 - e^{-\alpha 2 t})$, was used to curve fit the graph $f_D(t)$ as a function of time and determine the α_1 and α_2 coefficients needed to determine the RID functions.